Quasielastic Neutron Scattering from Soft Matter

Master Fundamental Physics and Applications

University of Orléans

Adapted from HERCULES lectures 2003/4

Gerald R. Kneller

Centre de Biophysique Moléculaire, CNRS
Rue Charles Sadron, F-45071 Orléans Cedex 2, France
and
Synchrotron SOLEIL
F-91192 Gif-sur-Yvette, France

Contents

CHAPTER 1

Information from neutron scattering

1. Introduction

This lecture gives an introduction into applications of quasielastic neutron scattering in the field of protein dynamics. It is by now a well established fact that molecular flexibility and dynamics play an essential role in the functioning of proteins. These properties depend, in turn, on temperature and hydration. A critical temperature for the physical functioning of some proteins seems to be the so-called glass-transition temperature at about 200 K. Below that temperature, the protein motion is essentially harmonic. Above 200 K, an additional stochastic component is seen in the dynamics, and at the same time the atomic fluctuations increase much more rapidly with temperature than below the transition temperature. The transition from one regime to the other is not very sharp, but takes place over a temperature range of some 10 Kelvin. W. DOSTER *et al.* studied the glass transition of myoglobin extensively by neutron scattering [**1**]. Recently CORDONE *et al.* demonstrated that myoglobin can be "frozen" in the harmonic state by immersing it in a trehalose solution [**2**]. Trehalose is a saccharide used by certain plants to protect themselves against extreme dryness. It conserves the plants in an inactive mode and allows them to recover normal functioning in a reversible way. A more direct relation between the glass transition temperature and protein function has been demonstrated by FERRAND *et al.* who showed that the photoactive membrane protein bacteriorhodopsin also undergoes a dynamic transition at a temperature [**3**] of about 220K, which is a critical temperature for the photo-activity of that protein: Below 220K bacteriorhodopsion cannot perform a complete photocycle. Finally, RASMUSSEN *et al.* showed by X-ray crystallography that ribonuclease looses its function below 220 K [**4**]. Exceeding the glass transition temperature is, however, not a necessary condition for the functioning of proteins. DANIEL *et al.* have shown that enzyme activity is not necessarily correlated with the transition temperature [**5**].

Thermal neutron scattering, which is sensitive to the dynamics and the structure of condensed matter on the atomic scale, gives very precise information about atomic fluctuations and dynamics in proteins. The energy of $k_B T$ at $T = 300\,K$ corresponds to a wavelength of 1.78 Å, which is the length scale of typical interatomic distances. The accessible time window is about 100 femtoseconds to 1 nanosecond, and the upper limit can be extended to

several 10 nanoseconds by spin-echo techniques. Compared to the enormous range of characteristic time scales of protein dynamics, which can extend up to a millisecond and more, this is still a relatively short time. Nevertheless, important dynamical processes, such as diffusion of small ligands in proteins, happen within this time window. Alternative and complementary techniques to neutron scattering are Mößbauer and Raman spectroscopy (see e.g. **[6]** for a recent application), far infrared spectroscopy, and NMR. From neutron scattering one obtains an *average view* of all atomic contributions. To analyze the complex spectra from proteins, one can use simple analytical models to understand essential features of the spectra. The internal dynamics is, however, too complex for a quantitative interpretation in terms of such models. Here computer simulations, and in particular Molecular Dynamics (MD) simulations, can help to gain more insight into the dynamics of proteins. Both methods access the same time and space domains, and the comparison of simulated and measured spectra is very direct, since neutrons are diffused by the atomic nuclei (neglecting magnetic scattering), which are the objects of MD simulations. Once an agreement between simulated and experimental spectra is found, the simulated trajectories can be analyzed in detail and information not accessible to experiments can be extracted from simulations **[7, 8, 9]**. Some recent applications concerning the simulation-based development of models for slow protein dynamics will be discussed in this lecture. They are relevant to the interpretation of quasielastic neutron scattering.

2. Neutron scattering theory

2.1. Properties of thermal neutrons. To be useful for research purposes, neutrons which have been produced by nuclear fission or by a spallation process must be slowed down to thermal energies. This is achieved by sending them through a moderator where they loose their initial energy in many collisions with the molecules of the moderator. After the moderation process the neutrons thus have typical energies of k_BT, where k_B is the Boltzmann constant ($1.381\,10^{-23} J/K$) and T the temperature in Kelvin. At $T = 300\,K$ the thermal energy is about $25\,meV$. The energy-momentum relationship of neutrons is that of non-relativistic particles,

$$E = \frac{\mathbf{p}^2}{2m}, \tag{1}$$

where $\mathbf{p}$ is the momentum and m is the neutron mass ($1.008\,a.m.u. = 1.674\,10^{-27} kg$). Using the relation between momentum and velocity, $\mathbf{p} = m\mathbf{v}$, we find $\mathbf{v}_{th} = 2285\,m/s$ as the velocity for thermal neutrons with an energy of $25\,meV$.

The Planck/De Broglie relationship yields a relation between the momentum, $\mathbf{p}$, and the wave vector, $\mathbf{k}$, of a neutron,

$$\mathbf{p} = \hbar\mathbf{k}, \tag{2}$$

$$\mathbf{k} = \frac{2\pi}{\lambda}\mathbf{n}, \qquad |\mathbf{n}| = 1. \tag{3}$$

Here $\hbar = h/2\pi$, $h = 6.626176\,Js$ is PLANCK'S constant, and $\mathbf{n}$ is a unit vector. We note that in quantum mechanics a particle with a sharply defined momentum is represented by a plane wave

$$\psi(\mathbf{r}, t) \propto \exp\left(\frac{i}{\hbar}(\mathbf{p}\cdot\mathbf{r} - Et)\right). \tag{4}$$

On account of the relations (2) and (3) the wavelength of a thermal neutron is found to be

$$\lambda = \frac{h}{\sqrt{2mE}} = 1.8\text{Å} \quad \text{for} \quad E = k_B T, \quad (T = 300K). \tag{5}$$

This means that the wave length of thermal neutrons is compatible with typical interatomic distances in condensed matter. Since the energy is comparable to the thermal energy of atoms in such systems, neutrons can be used to study the dynamics *and* the structure of condensed matter.

2.2. Dynamic structure factor. In neutron scattering experiments one measures the differential scattering cross section as a function of the energy and the momentum transfer on the sample **[10, 11]** (see Fig. 1). These quantities are denoted by $\Delta E = E_0 - E$ and $\Delta\mathbf{p} = \mathbf{p}_0 - \mathbf{p}$, respectively, where the index '0' refers to the incident neutrons. Usually the energy and momentum transfers as well as the momenta are expressed in units of $\hbar$, i.e.

$$\Delta E = \hbar\omega, \tag{6}$$

$$\Delta\mathbf{p} = \hbar(\mathbf{k}_0 - \mathbf{k}) = \hbar\mathbf{q}. \tag{7}$$

Using the above definitions of ω and $\mathbf{q}$, the differential scattering cross section can be cast into the form

$$\boxed{\frac{d^2\sigma}{d\Omega d\omega} = \frac{|\mathbf{k}|}{|\mathbf{k}_0|}\mathcal{S}(\mathbf{q},\omega)} \tag{8}$$

The function $\mathcal{S}(\mathbf{q},\omega)$ is called the *dynamic structure factor* and represents the quantity of interest in neutron scattering experiments. To understand which information it contains, we write it in the form

$$\boxed{\mathcal{S}(\mathbf{q},\omega) = \frac{1}{2\pi}\int_{-\infty}^{+\infty} dt\, \exp(-i\omega t)\mathcal{I}(\mathbf{q},t)} \tag{9}$$

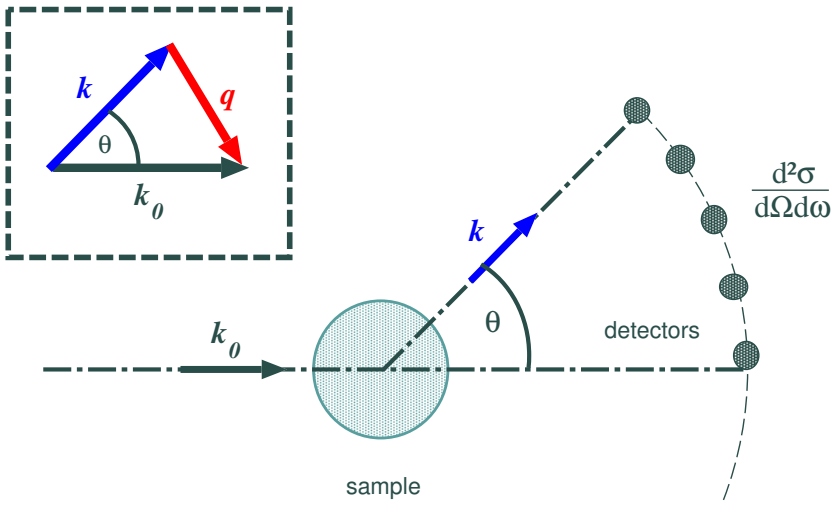

FIGURE 1. Sketch of a neutron scattering experiment. The neutrons hit the sample with an energy $E_0 = \hbar^2 \mathbf{k}_0^2/2m$ and leave it with $E = \hbar^2 \mathbf{k}^2/2m$ after the collision. The vectors $\mathbf{k}_0$ et $\mathbf{k}$ are the corresponding momenta in units of $\hbar$.

where $\mathcal{I}(\mathbf{q},t)$ is the *intermediate scattering function*. $\mathcal{I}(\mathbf{q},t)$ can be split into a *coherent* and an *incoherent part*,

$$\boxed{\mathcal{I}(\mathbf{q},t) = \mathcal{I}_{coh}(\mathbf{q},t) + \mathcal{I}_{inc}(\mathbf{q},t)}, \tag{10}$$

where $\mathcal{I}_{coh}(\mathbf{q},t)$ and $\mathcal{I}_{inc}(\mathbf{q},t)$ are defined as

$$\mathcal{I}_{coh}(\mathbf{q},t) = \sum_{\alpha,\beta} b_{\alpha,coh} b_{\beta,coh} \left\langle \exp\Big(i\mathbf{q}^T \cdot \mathbf{R}_\beta(t)\Big) \exp\Big(-i\mathbf{q}^T \cdot \mathbf{R}_\alpha(0)\Big) \right\rangle, \tag{11}$$

$$\mathcal{I}_{inc}(\mathbf{q},t) = \sum_{\alpha} b_{\alpha,inc}^2 \left\langle \exp\Big(i\mathbf{q}^T \cdot \mathbf{R}_\alpha(t)\Big) \exp\Big(-i\mathbf{q}^T \cdot \mathbf{R}_\alpha(0)\Big) \right\rangle, \tag{12}$$

respectively. The symbol $\langle \ldots \rangle$ denotes a quantum statistical average over a thermodynamic ensemble, and $\mathbf{R}_\alpha$ is the position operator of atom α. The quantities $b_{\alpha,coh}$ et $b_{\alpha,inc}$ are the coherent and incoherent scattering length, respectively, of atom α. They have values of the order of a fm ($1\,fm = 10^{-15}\,m$), which is about the size of an atomic nucleus. The *total scattering cross section* of atom α is given by

$$\sigma_{\alpha,tot} = 4\pi \left(b_{\alpha,coh}^2 + b_{\alpha,inc}^2\right), \tag{13}$$

and refers to a *bound* atom.

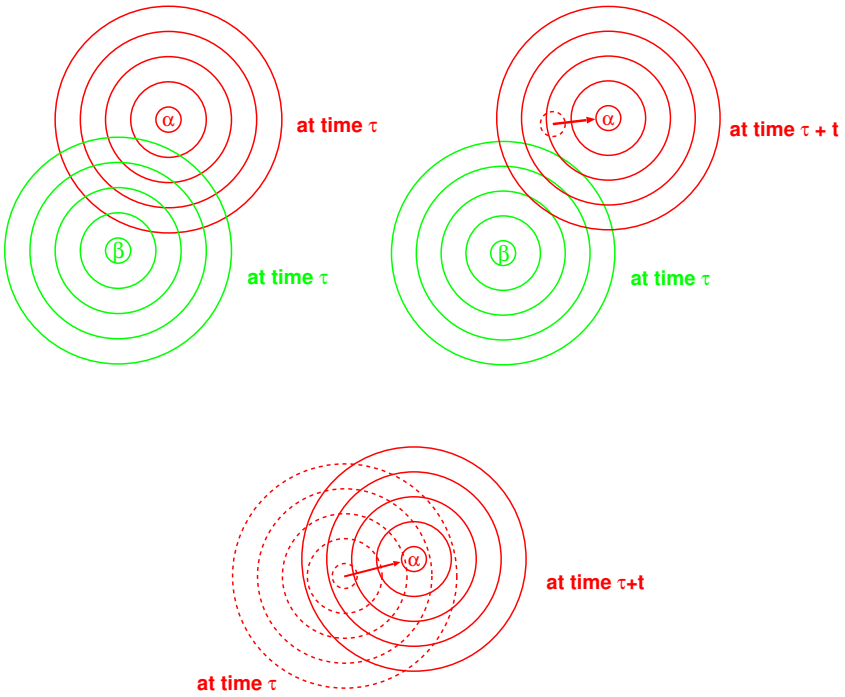

FIGURE 2. **Upper left:** Interference of neutron waves emitted from different atoms at the same time (coherent elastic scattering = diffraction). **Upper right:** Interference of neutron waves emitted from different atoms at different times (coherent inelastic scattering). **Lower:** Interference of neutron waves emitted from the *same* atom at different times (incoherent inelastic scattering).

It should be noted that $\mathcal{I}_{inc}(\mathbf{q},t)$ describes only self-correlations between atomic positions, whereas $\mathcal{I}_{coh}(\mathbf{q},t)$ describes also cross-correlations due to *collective motions* – see Fig. 2. It is important to note that the accessible $(|\mathbf{q}|,\omega)$-range is determined by the relation between momentum and energy (dispersion relation). To keep the notation simple we introduce

$$q := |\mathbf{q}| = \sqrt{q_x^2 + q_y^2 + q_z^2} \tag{14}$$

for the modulus of the momentum transfer. It follows from (1) and (2) that

$$E = \frac{\hbar^2 \mathbf{k}^2}{2m} = \frac{\hbar^2 {\mathbf{k}_0}^2}{2m} - \hbar\omega. \tag{15}$$

Therefore

$$q = k_0 \sqrt{2 - \frac{\hbar\omega}{E_0} - 2\sqrt{1 - \frac{\hbar\omega}{E_0}}\cos\theta}. \tag{16}$$

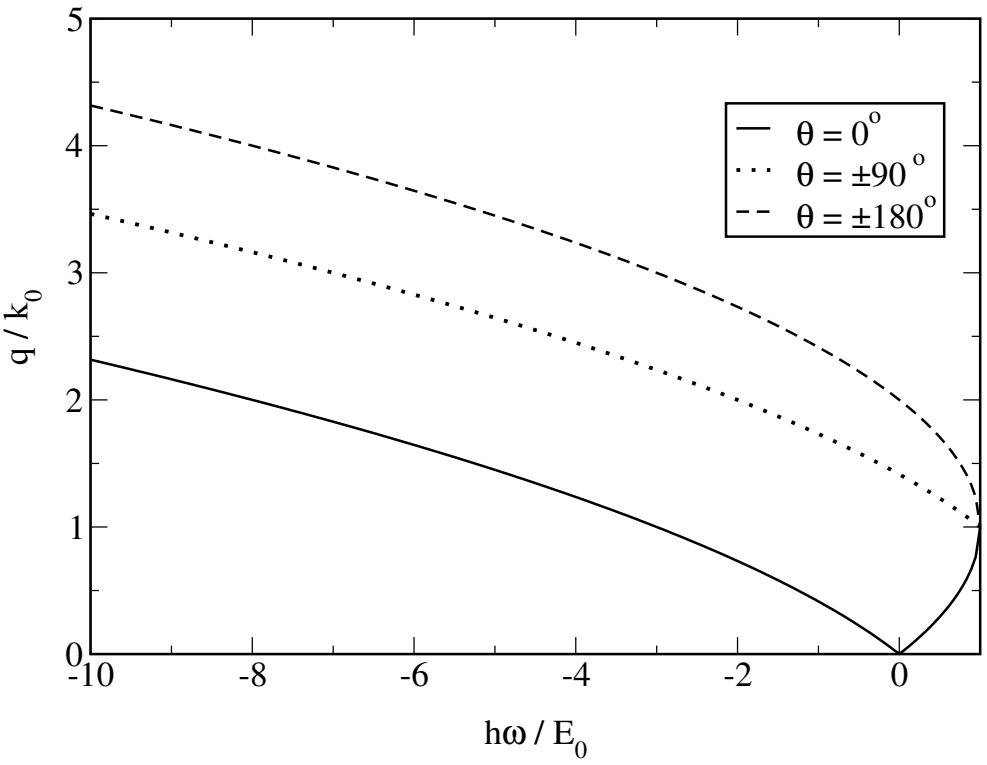

FIGURE 3. Accessible (q, ω)-range for a given initial energy, E_0. Depicted is the relation between q/k_0 and $\hbar\omega/E_0$ for $\theta = \{0, \pm\frac{\pi}{2}, \pm\pi\}$. Note that $q(\theta, \omega)$ is even in θ (see eq. 16).

For a given scattering angle θ, the momentum transfer q is a function of ω (see Fig. 3). Since the energy loss of the neutrons cannot exceed their initial energy, E_0, it follows that $E_0/\hbar$ is an upper limit for ω.

2.3. Detailed balance and classical limit. Since $\mathcal{I}(\mathbf{q}, t)$ is a time correlation whose time evolution follows the laws of quantum mechanics, the dynamic structure factor is not symmetric in ω. Energy loss of the neutron is preferred to energy gain **[11, 10]**,

$$\boxed{\mathcal{S}(\mathbf{q}, \omega) = \exp\left(\frac{\hbar\omega}{k_B T}\right) \mathcal{S}(-\mathbf{q}, -\omega)} \tag{17}$$

We recall that $\hbar\omega > 0$ is an energy gain of the sample and therefore an energy loss of the neutron. Usually one replaces the intermediate scattering function by its classical counter part – i.e. a classical time correlation function – if the sample under consideration can be described in terms of classical mechanics. This procedure consists in passing formally $\hbar$ to zero. As a result the resulting

dynamic structure factor fulfills

$$\boxed{\mathcal{S}_{cl}(\mathbf{q},\omega) = \mathcal{S}_{cl}(-\mathbf{q},-\omega)} \tag{18}$$

It has been shown in **[12]** that the quantum time correlation function defining $\mathcal{I}(\mathbf{q},t)$ is not to be replaced by its classical counterpart if the scattering system is described by classical mechanics. Essentially the mathematical limit $\hbar \to 0$ leads to neglecting the kinematic effects of the momentum transfer $\hbar\mathbf{q}$ from the neutron to the sample. Only if

$$\boxed{\frac{\hbar^2 q^2}{2M} \ll k_B T} \tag{19}$$

where M is the effective mass of the scattering atom, $\mathcal{S}_{cl}(\mathbf{q},\omega)$ describes neutron scattering from classical systems and one can approximate

$$\mathcal{I}_{coh}(\mathbf{q},t) \approx \sum_{\alpha,\beta} b_{\alpha,coh} b_{\beta,coh} \left\langle \exp\Big(i\mathbf{q}^T \cdot [\mathbf{R}_\beta(t) - \mathbf{R}_\alpha(0)]\Big)\right\rangle, \tag{20}$$

$$\mathcal{I}_{inc}(\mathbf{q},t) \approx \sum_{\alpha} b^2_{\alpha,inc} \left\langle \exp\Big(i\mathbf{q}^T \cdot [\mathbf{R}_\alpha(t) - \mathbf{R}_\alpha(0)]\Big)\right\rangle. \tag{21}$$

Here $\{\mathbf{R}_\alpha(t)\}$ are real-valued vectors and not operators anymore. The classical approximation will be made in the following.

2.4. Incoherent scattering. If one considers a sample containing a large proportion of hydrogen atoms one can approximate

$$\boxed{\mathcal{I}(\mathbf{q},t) \approx N\, b^2_{H,inc} I_H(\mathbf{q},t)} \tag{22}$$

where N is the number of hydrogen atoms in the sample, $b_{H,inc}$ is the incoherent scattering length of hydrogen, and

$$\boxed{I_H(\mathbf{q},t) = \frac{1}{N} \sum_{\alpha\in\{H\}} \left\langle \exp\Big(i\mathbf{q}^T \cdot [\mathbf{R}_\alpha(t) - \mathbf{R}_\alpha(0)]\Big)\right\rangle} \tag{23}$$

Correspondingly we define the dynamic structure factor

$$\boxed{S_H(\mathbf{q},\omega) = \frac{1}{2\pi} \int_{-\infty}^{+\infty} dt\, \exp(-i\omega t) I_H(\mathbf{q},t)} \tag{24}$$

Table 1 shows that approximation (22) can be made since incoherent scattering from hydrogen atoms dominates all other scattering processes. This fact allows to mask certain parts of a system under consideration by *partial deuteration*. If one studies for example a ("normal", hydrogenated) protein in a deuterated solution, the solvent contribution is strongly reduced and one measures essentially self-correlations of the hydrogen positions in the protein. Hydrogen atoms in a protein are homogeneously distributed, and neutron scattering

Element	H	D	C	O	N	S
b_{coh}	-3.741	6.674	6.648	5.805	9.300	2.847
b_{inc}	$\boxed{25.217}$	4.022	0.285	0.000	2.241	0.188

TABLE 1. Scattering lengths of some elements in fm ($10^{-15}\,m$).

experiments thus give an *averaged view* of protein dynamics. So far most neutron scattering experiments with proteins have been made with hydrogenated proteins, either in D_2O-solutions or in D_2O-hydrated powders. Experiments with powders have been quite popular in the past since they prevent global protein translations and rotations, which make the analysis of neutron scattering spectra difficult.

To understand better which information can be obtained from incoherent neutron scattering, it is convenient to introduce the van Hove self-correlation function **[13]** via

$$G_H(\mathbf{r},t) = \frac{1}{(2\pi)^3}\int d^3q\, \exp(-i\mathbf{q}^T\cdot\mathbf{r}) I_H(\mathbf{q},t). \tag{25}$$

Defining the single particle density,

$$\rho_\alpha(\mathbf{r},t) := \delta\left(\mathbf{r}-\mathbf{R}_\alpha(t)\right), \tag{26}$$

one can write

$$G_H(\mathbf{r},t) = \frac{1}{N_H}\sum_{\alpha\in\{H\}} G_{\alpha\alpha}(\mathbf{r},t), \tag{27}$$

$$G_{\alpha\alpha}(\mathbf{r},t) = \int d^3r'\ \langle\rho_\alpha(\mathbf{r}+\mathbf{r}',t)\rho_\alpha(\mathbf{r}',0)\rangle\,. \tag{28}$$

Definition (28) is closely relation to the "Patterson form" of the intensity of a diffracted X-ray wave in crystallography. The introduction of van Hove correlation functions is only useful in the classical limit (which we consider in this lecture). In this case one can write

$$G^{cl}_{\alpha\alpha}(\mathbf{r},t) = \langle\delta\left(\mathbf{r}-[\mathbf{R}_\alpha(t)-\mathbf{R}_\alpha(0)]\right)\rangle\,, \tag{29}$$

and the van Hove self-correlation function $G^{cl}_{\alpha\alpha}(\mathbf{r},t)$ can be interpreted as *probability density for a displacement* $\mathbf{r}$ *of atom* α *within time* t.

2.5. Elastic Incoherent Structure Factor. In many cases the samples used for studies of protein dynamics were hydrated powders. In such a system translations and rotations of a whole protein are blocked and neutrons see then only *internal* motions of proteins. The latter are by definition confined in space, and $\lim_{t\to\infty} G_H(\mathbf{r},t)$ takes a finite value – in a very rough approximation the

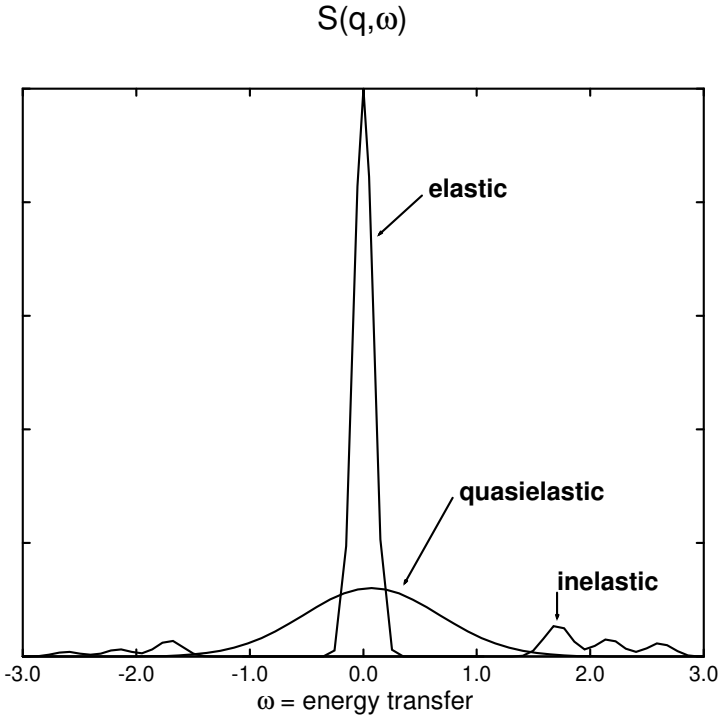

FIGURE 4. Sketch of an incoherent neutron scattering spectrum. Due to finite instrumental resolution the elastic line has always finite width.

inverse of the average volume explored in configuration space. Consequently, the intermediate scattering function tends to a plateau value, too,

$$\boxed{EISF(\mathbf{q}) = \lim_{t\to\infty} I_H(\mathbf{q},t) = \int d^3r\ \exp(i\mathbf{q}^T\cdot\mathbf{r}) G_H(\mathbf{q},\infty)} \tag{30}$$

This plateau value is called the *Elastic Incoherent Structure Factor* (EISF). The name becomes clear if we consider the dynamic structure factor. Defining

$$I'_H(\mathbf{q},t) = I_H(\mathbf{q},t) - I_H(\mathbf{q},\infty), \tag{31}$$

one can write

$$\boxed{S_H(\mathbf{q},\omega) = EISF(\mathbf{q})\delta(\omega) + S'_H(\mathbf{q},\omega)} \tag{32}$$

The component $S'_H(\mathbf{q},\omega)$ contains the *quasielastic spectrum*, which is centered on $\omega = 0$ and describes stochastic motions, and the *inelastic spectrum*, which is due to vibrational motions (see Fig. 4). The symbol $\delta(\omega)$ stands for a Dirac distribution and represents an ideal elastic line of zero width and finite integral. One possible representation is a normalized Gaussian in the limit of zero

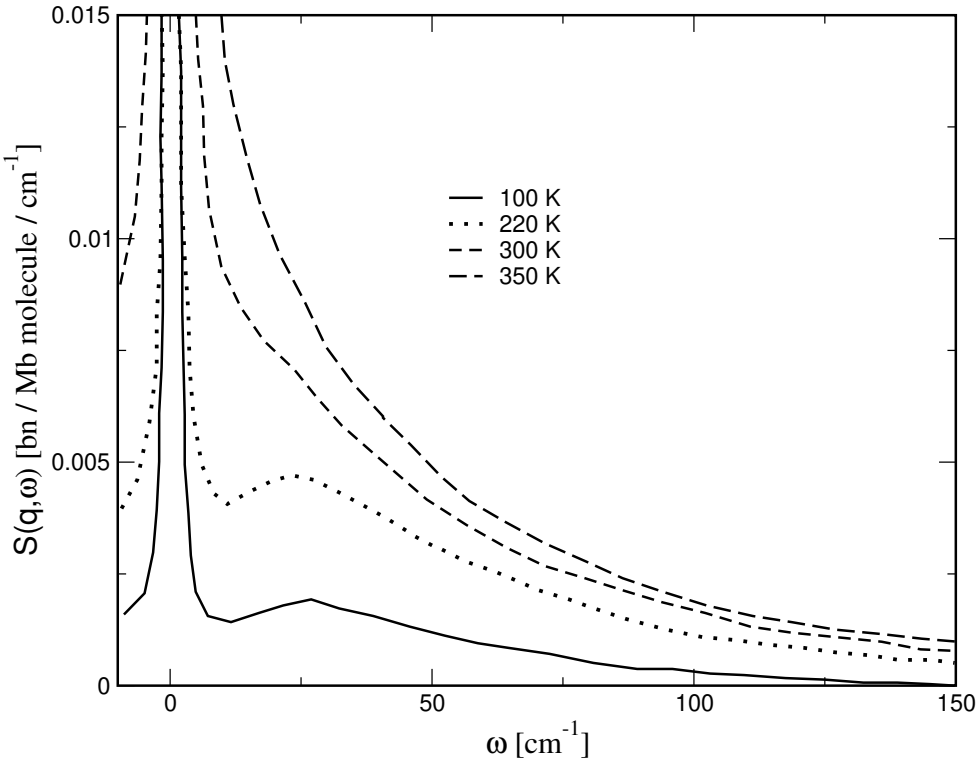

FIGURE 5. Temperature dependence of $S(q,\omega)$ for D_2O-hydrated myoglobin powders from ref. **[14]** (data re-plotted). The data are shown for a mean scattering angle of $108.3°$. At low temperatures one sees a "Boson-peak" at about 25 cm^{-1}.

width,

$$\delta(\omega) = \frac{1}{2\pi}\int_{-\infty}^{+\infty} dt\ \exp(-i\omega t) = \lim_{\epsilon\to 0}\frac{1}{\sqrt{2\pi}\epsilon}\exp\left(-\frac{\omega^2}{2\epsilon^2}\right). \tag{33}$$

The $EISF$ is an important quantity since it gives a first idea about the characteristics of the dynamical processes in the scattering system. It follows from definition (24) of $S_H(\mathbf{q},\omega)$ that $\int_{-\infty}^{+\infty} d\omega\, S_H(\mathbf{q},\omega) = I_H(\mathbf{q},0) = 1$. Using (32) we therefore obtain

$$\boxed{EISF(\mathbf{q}) + \int_{-\infty}^{+\infty} d\omega\, S'_H(\mathbf{q},\omega) = 1} \tag{34}$$

This is a "sum rule", saying that any dynamical process yielding a contribution to $S'_H(\mathbf{q},\omega)$ leads to a drop-off in the $EISF$.

Finally, we note that the EISF can also be written in the form

$$\boxed{EISF(\mathbf{q}) = \frac{1}{N_H}\sum_{\alpha\in\{H\}}\left|\left\langle\exp\left(-i\mathbf{q}^T\cdot\mathbf{R}_\alpha\right)\right\rangle\right|^2} \tag{35}$$

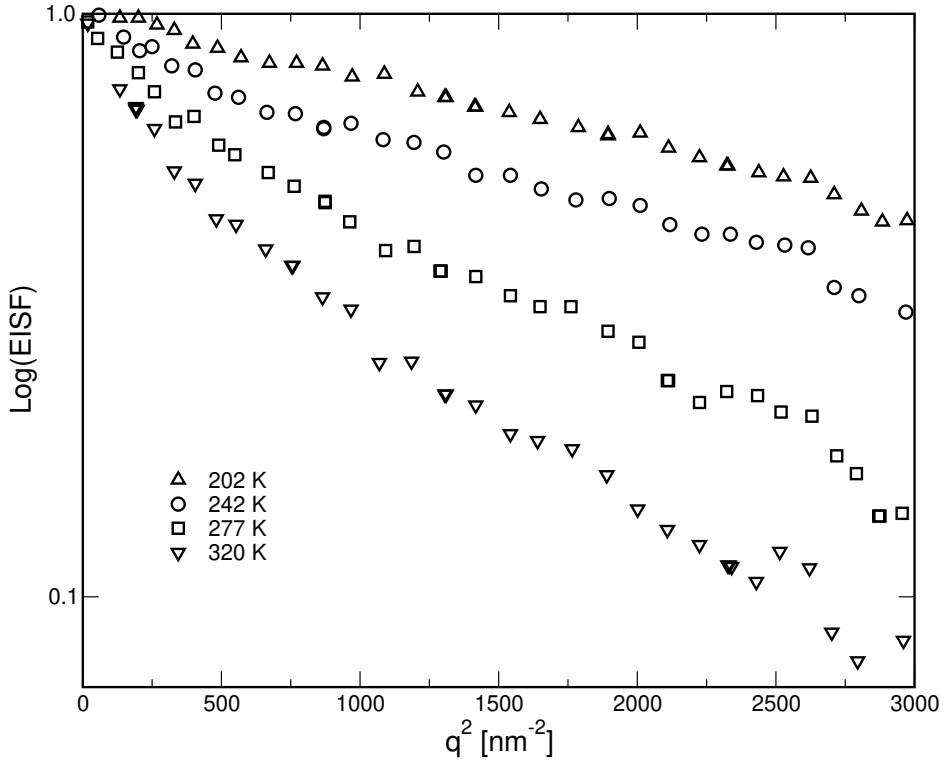

FIGURE 6. Normalized elastic intensity of D_2O-deuterated myoglobin at 202 K (triangles up), 242 K (circles), 277 K (squares) d) 320 K (triangles down). The data are re-plotted from ref. [**15**].

Here one makes use of the fact that the motions of an atom become uncorrelated in the limit of an infinite time lag.

2.6. Motion types. In order to able to analyse the data from quasi- and inelastic neutron scattering in terms of models for different motion types the motion of the atoms in the sample need to be decomposed in the form

$$\mathbf{R}_\alpha = \mathbf{R}_{CM} + \mathbf{r}_\alpha + \mathbf{u}_\alpha. \tag{36}$$

Here $\mathbf{R}_{CM}$ is the position of the center-of-mass of a tagged protein, $\mathbf{r}_\alpha$ is the position of atom α relative to the center-of-mass, with $|\mathbf{r}_\alpha| = const.$, and $\mathbf{u}_\alpha$ describes motions around $\mathbf{R}_{CM} + \mathbf{r}_\alpha$. The basic assumptions are now that the motions of $\mathbf{R}_{CM}$, $\mathbf{r}_\alpha$, and $\mathbf{u}_\alpha$ are *uncorrelated* and that all atoms can be considered as *equivalent*. More precisely, we consider a tagged protein molecule, and $\mathbf{R} = \mathbf{R}_{CM} + \mathbf{r} + \mathbf{u}$ is the position of a "representative atom" in that protein molecule. Formally, such a description is valid only for small and highly symmetric molecules such as methane (CH_4). In more complicated systems this

picture cannot be maintained and a tagged atom should be thought of as a "model atom" having the average properties of the scattering atoms.

Making the above assumptions, the intermediate scattering function $I(\mathbf{q},t)$ can be factorized as [1]

$$\boxed{I(\mathbf{q},t) = I_{CM}(\mathbf{q},t)I_{rot}(\mathbf{q},t)I_{int}(\mathbf{q},t)} \tag{37}$$

where

$$I_{CM}(\mathbf{q},t) = \langle \exp(i\mathbf{q}^T \cdot [\mathbf{R}_{CM}(t) - \mathbf{R}_{CM}(0)]) \rangle, \tag{38}$$

$$I_{rot}(\mathbf{q},t) = \langle \exp(i\mathbf{q}^T \cdot [\mathbf{r}(t) - \mathbf{r}(0)]) \rangle, \tag{39}$$

$$I_{int}(\mathbf{q},t) = \langle \exp(i\mathbf{q}^T [\mathbf{u}(t) - \mathbf{u}(0)]) \rangle. \tag{40}$$

The indices "rot" and "int" refer to rotational and internal motions, respectively. The latter are often identified with vibrations, but they may as well describe diffusive motions which are confined in space. Protein atoms in hydrated protein powders perform such motions. An immediate consequence of (37) is that $S_H(\mathbf{q},\omega)$ is a convolution product[2] in frequency space of the form

$$\boxed{S(\mathbf{q},\omega) = (S_{CM} * S_{rot} * S_{int})(\mathbf{q},\omega)} \tag{41}$$

In such a convolution product each "factor" produces a broadening of the spectrum. If each contribution could be represented by a Gaussian, the total width would be the sum of the widths of the individual contributions.

2.7. Gaussian approximation. In the following we will discuss the Gaussian approximation (GA) of the incoherent scattering function. In practice the latter concerns essentially *internal motions*. This point will be come clear in the next chapter when analytical models for protein dynamics will be discussed. In order to simplify the formulae we will chose $\mathbf{q} = q\mathbf{e}_x$, and, for simplicity we consider only *one* single atom. The GA for an ensemble of atoms is straightforward. When the GA is used for analytical models the chosen atom is a sort of "representative atom" for the dynamics of all hydrogen atoms in the system. In this case one makes a second severe approximation, writing $\mathcal{I}(\mathbf{q},t) = N_H b_{H,inc}^2 I(q,t)$, where $I(q,t)$ describes the dynamics of a tagged hydrogen atom. Keeping the above remarks in mind, we start from the intermediate scattering function

$$I(q,t) = \langle \exp(iq[x(t) - x(0)]) \rangle \,. \tag{42}$$

With the definition

$$d(t) = x(t) - x(0) \tag{43}$$

[1] In the following we omit the subscript 'H'.

[2] The definition of the convolution of two functions is $(f * g)(x) = \int_{-\infty}^{+\infty} dy\, f(x-y)g(y)$.

the function $I(q,t)$ can be written as a cumulant expansion **[16, 17]**,

$$\boxed{I(q,t) = \exp\left(-q^2\rho_1(t) + q^4\rho_2(t) - q^6\rho_3(t) + \ldots\right)} \tag{44}$$

The first few terms $\rho_k(t)$ are given by

$$\rho_1(t) = \frac{1}{2!}\langle d^2(t)\rangle, \tag{45}$$

$$\rho_2(t) = \frac{1}{4!}\left(\langle d^4(t)\rangle - 3\langle d^2(t)\rangle^2\right), \tag{46}$$

$$\rho_3(t) = \frac{1}{6!}\left(\langle d^6(t)\rangle - 15\langle d^4(t)\rangle\langle d^2(t)\rangle + 30\langle d^2(t)\rangle^2\right). \tag{47}$$

We note that

$$\boxed{W_x(t) \equiv \langle[x(t) - x(0)]^2\rangle = 2\,\rho_1(t)} \tag{48}$$

is the *mean square displacement* of the selected atom in x-direction. In an isotropic system we have $W_x(t) = W_y(t) = W_y(t)$. Defining

$$\boxed{W(t) = \langle[\mathbf{R}(t) - \mathbf{R}(0)]^2\rangle = W_x(t) + W_y(t) + W_z(t)} \tag{49}$$

definitions the GA can thus be written as

$$\boxed{I(q,t) \approx \exp\left(-\frac{q^2}{6}W(t)\right)} \tag{50}$$

If the motions of the representative atom are confined in space the MSD tends towards a plateau value for $t \to \infty$ (see e.g. relation (108)),

$$\boxed{\lim_{t\to\infty} W(t) = 2\,\langle\mathbf{R}^2\rangle} \tag{51}$$

In the GA the EISF thus has a particularly simple form:

$$\boxed{EISF(q) = \lim_{t\to\infty} I(q,t) \approx \exp\left(-\frac{q^2}{3}\langle\mathbf{R}^2\rangle\right)} \tag{52}$$

It follows from the cumulant expression (44) that the GA is always a good approximation for small q, independent of the forces acting on the tagged atom.

3. Examples

3.1. Neutron scattering from hydrated myoglobin powders. Let us now consider elastic and quasielastic scattering from D_2O-hydrated myoglobin powders as an example to illustrate the sum rule (34) for the EISF. For this purpose we use data from CUSACK & DOSTER **[14]** and from DOSTER *et al.* **[15]**. Since the heme group of myoglobin contains an iron atom, the internal dynamics of this protein has been studied quite early by Mößbauer spectroscopy

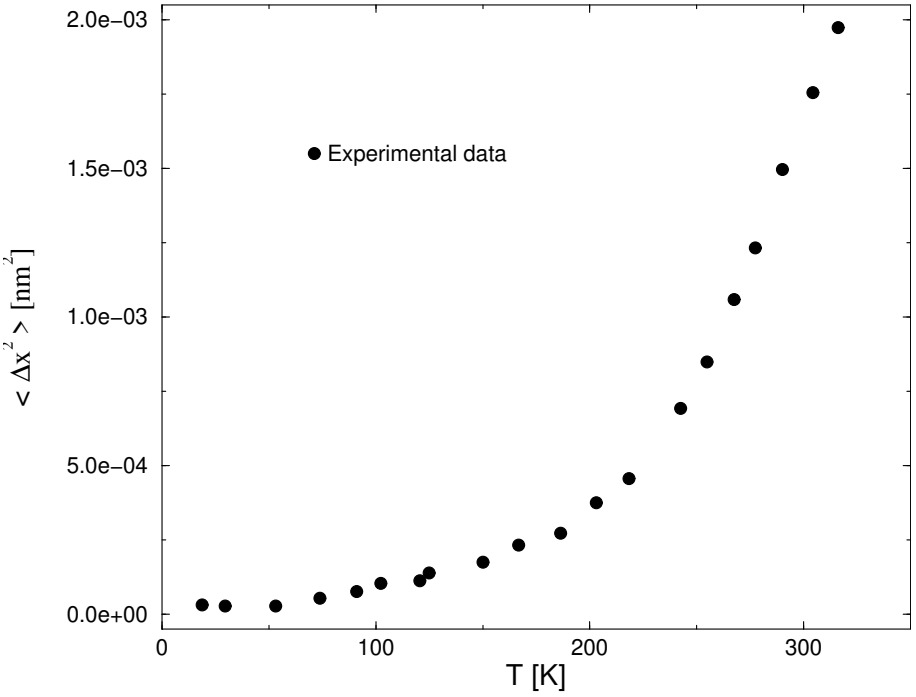

FIGURE 7. Position fluctuations of hydrogen atoms in myoglobin as a function of temperature [**1**].

(see [**18**] and references cited herein). Later DOSTER, CUSACK and co-workers stayed with myoglobin, using however neutron scattering.

Since the atomic motions in powders are confined in space, the $EISF$ does not vanish. Fig. 5 shows $S(q,\omega)$ for D_2O-hydrated myoglobin powders at different temperatures. With increasing temperature the quasielastic line becomes broader, and, according to the sum rule (34), one should expect that the $EISF$ drops off. This is indeed the case, as can be seen from Fig. 6. It should be noted that $S(q,\omega)$ in Fig. 5 is not given for a specific value of q, but for an average value of the scattering angle θ (see Fig. 3).

3.2. Elastic scans and glass transition. Expression (52) is often used to to analyze "elastic scans" of protein powders, tracing $\ln(EISF)$ versus q^2. Within the Gaussian approximation the slope of $\ln(EISF)$ yields thus an estimation of the mean square position fluctuation, $\langle x^2 \rangle$. Tracing the latter versus temperature allows to localise the dynamic transition ("glass transition") seen in many proteins at around 200 K – see Figs. 7 and 8. This dynamic transition is characterized by an abrupt change of the slope of the position fluctuations plotted versus temperature. For low temperatures the position fluctuations grow approximately linearly with temperature, which is characteristic for harmonic

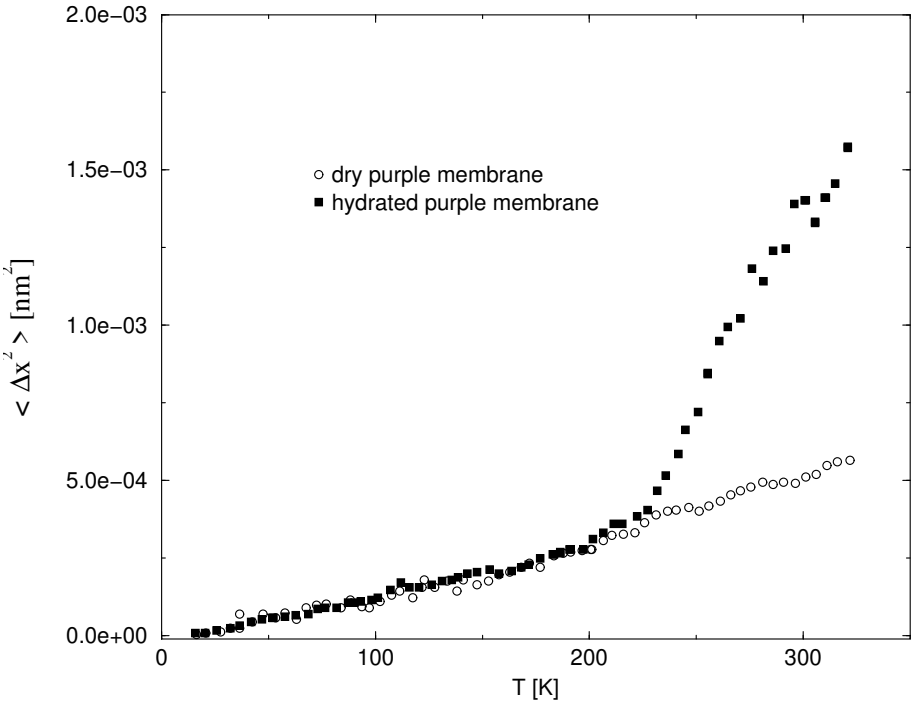

FIGURE 8. Position fluctuations of the hydrogen atoms in bacteriorhodopsin (BR) as a function of temperature and hydration [**3**]. For BR in the dry membrane the EISF exhibits a harmonic behavior over the whole temperature range, whereas for BR in the hydrated membrane a dynamic transition is seen at around 220 K. This dynamic transition is correlated with the function of BR as a "proton pump".

behavior. This point will become clear when we will discuss the Langevin oscillator as a simple model for the motion of atoms in a protein. The abrupt change in slope is identified with "anharmonic behavior", but as we will see later, one may also consider that the dynamics above the transition temperature is characterized by an *effective* harmonic potential with smaller curvature.

3.3. Quasielastic scattering from lysozyme in solution. . The last example show data from a recent study of lysozyme in *solution* using the high resolution time-of-flight spectrometer IN5 at the Institut Laue-Langevin in Grenoble [**19**]. The solvent was a deuterated acetate buffer (50mM and pH4.6) whose condition favours the monomeric form of lysozyme. The usage of a deuterated solution increases the contrast between the lysozyme molecules and the solution, which is not the object of interest in the presented study. In order to minimise the risk of aggregation the protein concentration was chosen to be 60 mg/ml. This concentration leaves still a sufficient amount of protein for the

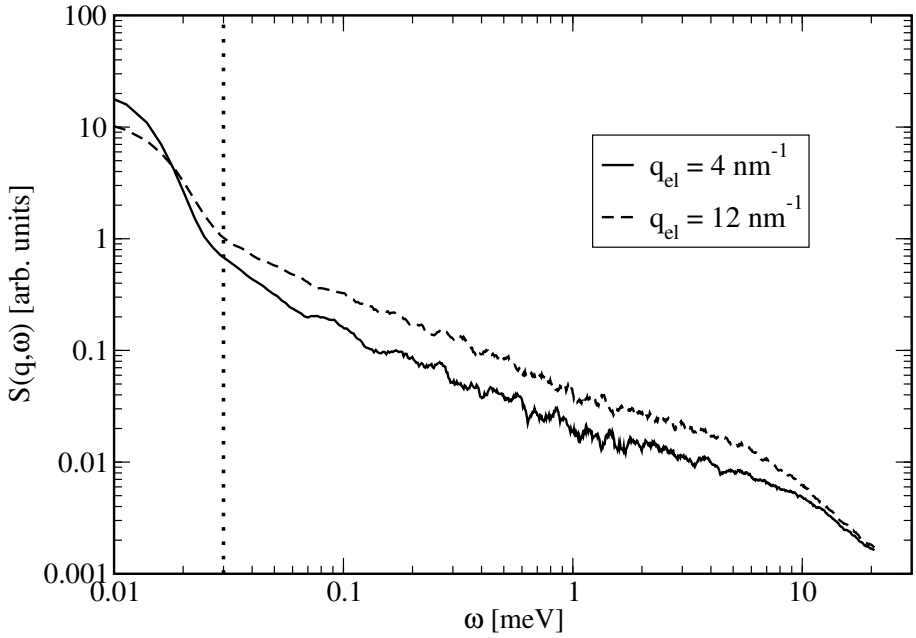

FIGURE 9. Log-log plot of the quasielastic neutron scattering spectrum of lysozym in a deuterated solution. The data have been obtained from the IN5 spectrometer at the Institut Laue-Langevin in Grenoble [**19**]. The vertical broken line indicates the point on the frequency axis where the EISF-weighted contribution due to global diffusion and instrumental resolution becomes dominant – see details in the text.

scattering experiments. Figure 9 shows the scattering intensities of the protein for $q_{el} = 0.4\,\text{Å}^{-1}$ and $q_{el} = 1.2\,\text{Å}^{-1}$. For energy transfers smaller than about $0.03\,meV$ the influence of instrumental resolution and global diffusion of the lysozyme molecules become visible. To understand this point we account first for the finite resolution of the instrument, writing

$$S_{meas}(\mathbf{q},\omega) = (R * S)(\mathbf{q},\omega). \tag{53}$$

Here $R(\omega)$ is the resolution function of the instrument. We note that the latter may also be a function of the momentum transfer $\mathbf{q}$. The index "*meas*" stands for "measured". If we assume that global and internal motions of proteins are uncorrelated, we can write

$$S(\mathbf{q},\omega) = (S_g * S_{int})(\mathbf{q},\omega), \tag{54}$$

where $S_g(\mathbf{q},\omega)$ describes the global motions, i.e. translations and rotations of whole proteins. Assuming that translational and rotational motions are also uncorrelated, $S_g(\mathbf{q},\omega)$ is itself a convolution product,

$$S_g(\mathbf{q},\omega) = (S_{CM} * S_{rot})(\mathbf{q},\omega). \tag{55}$$

Since the EISF of internal protein motions is non-zero, we can use expression (32) and write (we omit the index "H")

$$\boxed{S(\mathbf{q},\omega) = EISF(\mathbf{q})S_g(\mathbf{q},\omega) + (S_g * S')(\mathbf{q},\omega)}. \tag{56}$$

Using that the above expression is to be convoluted with the resolution function in order to obtain the measured spectrum, we get from (53)

$$\boxed{S_{meas}(\mathbf{q},\omega) = EISF(\mathbf{q})(R * S_g)(\mathbf{q},\omega) + (R * S_g * S')(\mathbf{q},\omega)}. \tag{57}$$

The hump at smaller energy transfers which is seen in Fig. 9 is due to the EISF-weighted contribution to the spectrum which represents the (resolution-broadened) spectrum of global diffusion. The remaining spectrum describes predominantly internal protein dynamics which is characterised by a broad spectrum of relaxation rates. A simulation-based theoretical model will be developed at the end of the lecture.

CHAPTER 2

Analytical models for $I(q,t)$

1. Introducing dynamical models

In the following the expression "particle" can refer to quite different physical objects. It may design a whole protein or simply a tagged "representative" atom in a protein. The state of the system under consideration may be defined by a set of f parameters, $\Omega \equiv \{\Omega_i\}$ ($f = 1, \ldots, f$). To express spectroscopic quantities like neutron scattering spectra we need the *joint probability density* $P(\Omega, t; \Omega', t')$ for finding the system at time t' in state Ω' and at time $t > t'$ in state Ω. Using Baye's rule one can write

$$\boxed{P(\Omega, t; \Omega', t') = P(\Omega, t|\Omega', t')P(\Omega', t')} \tag{58}$$

where $P(\Omega, t|\Omega', t')$ is the *conditional probability density* to find the system in state Ω at time t, given it was in state Ω' at time t'. The quantity $P(\Omega', t')$ is the probability density for finding the system at time t' in state Ω'. If the system is in equilibrium we may write $P(\Omega, t|\Omega', t') = P(\Omega, t - t'|\Omega', 0)$ and $P(\Omega', t') = P_{eq}(\Omega')$ is the equilibrium density. The latter is related to the conditional probability density by

$$\boxed{P_{eq}(\Omega) = \lim_{t\to\infty} P(\Omega, t|\Omega', t')} \tag{59}$$

In the following we consider systems in equilibrium and set $t' = 0$. With the above definitions the intermediate scattering function takes the form

$$\boxed{I(\mathbf{q}, t) = \int\int d\Omega d\Omega'\, P(\Omega, t; \Omega', t') \exp\Big(i\mathbf{q} \cdot [\mathbf{R}(\Omega) - \mathbf{R}(\Omega')]\Big)} \tag{60}$$

and the van Hove function reads correspondingly

$$\boxed{G(\mathbf{r}, t) = \int\int d\Omega d\Omega'\, P(\Omega, t; \Omega', t')\delta\left(\mathbf{r} - [\mathbf{R}(\Omega) - \mathbf{R}(\Omega')]\right)} \tag{61}$$

In (60) and (61) the joint probability density, $P(\Omega, t; \Omega', t')$, is written in the form (58) and a dynamical model is introduced for the *conditional* probability density. The evolution of the latter is determined by a partial differential equation following from the dynamical model,

$$\boxed{\partial_t P = \hat{\mathcal{L}}_\Omega P; \qquad P(\Omega, 0|\Omega', 0) = \delta(\Omega - \Omega')} \tag{62}$$

Here $\hat{\mathcal{L}}_\Omega$ is a differential operator acting on the variables Ω.

2. Global motions

In the following we will discuss two models which are used to describe the translational and rotational motions of whole molecules. They are applicable to diluted solutions and spherical molecules in the case of rotational motion.

2.1. Translational diffusion. Let us first consider the translational motion of whole protein molecules immersed in a viscous solvent like water. Here one can assume that the molecules undergo diffusional motion on a coarse-grained time scale considerably longer than the velocity relaxation time of the solvent molecules. This type of motion is known as Brownian motion. If the protein concentration is lower than about 5 % volume fraction, hydrodynamic interactions between the protein molecules can be neglected and it is sufficient to consider a single molecule. The state of the system is thus simply described by the three Cartesian coordinates of the tagged molecule, $\Omega \equiv \{x, y, z\}$, and $\mathbf{R} = (x, y, z)^T$ is position vector of its center of mass. The time evolution of $P(\mathbf{R}, t|\mathbf{R}', 0)$ is described by the *diffusion equation*,

$$\boxed{\partial_t P = D\left(\frac{\partial^2}{\partial x^2} + \frac{\partial^2}{\partial y^2} + \frac{\partial^2}{\partial z^2}\right) P} \tag{63}$$

Here D is the translational diffusion constant which has the dimension m^2/s in SI units. The diffusion equation (63) is to be solved with the initial condition

$$P(\mathbf{R}, 0|\mathbf{R}', 0) = \delta(\mathbf{R} - \mathbf{R}'). \tag{64}$$

The solution of (63) has Gaussian shape in $\mathbf{R}$,

$$P(\mathbf{R}, t|\mathbf{R}', 0) = \frac{1}{\sqrt{4\pi D t}^3} \exp\left(-\frac{|\mathbf{R} - \mathbf{R}'|^2}{4Dt}\right), \tag{65}$$

and the equilibrium distribution is here simply

$$P_{eq}(\mathbf{R}) = \frac{1}{V}, \tag{66}$$

where V is a macroscopic integration volume.

Using Eq. (60), the intermediate scattering function takes the form

$$\boxed{I(\mathbf{q}, t) = \exp(-Dq^2 t)} \tag{67}$$

and the corresponding van Hove function is obtained from[1] (61),

$$\boxed{G(\mathbf{r}, t) = \frac{1}{\sqrt{4\pi D t}^3} \exp\left(-\frac{r^2}{4Dt}\right)} \tag{68}$$

[1] $r := \|\mathbf{r}\| = \sqrt{x^2 + y^2 + z^2}$.

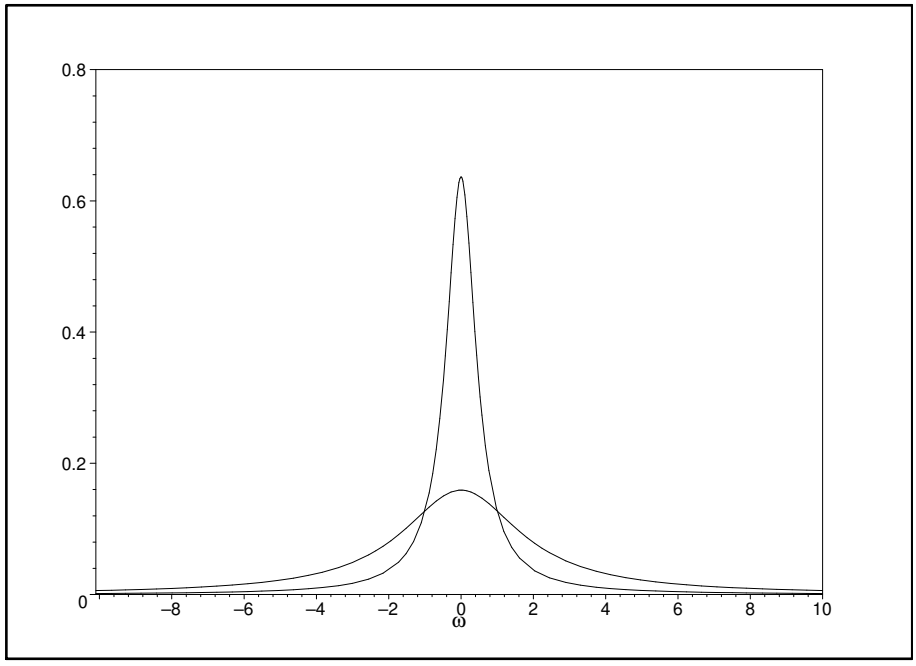

FIGURE 1. Form of $S(\mathbf{q},\omega)$ for translational diffusion. The widths of the the two Lorentzian profiles (on the ω-scale) are $\Gamma = 0.5$ (narrow line) and $\Gamma = 2$.

If expression (67) is Fourier transformed with respect to time we obtain the dynamic structure factor,

$$\boxed{S(\mathbf{q},\omega) = \frac{1}{\pi}\frac{Dq^2}{\left(Dq^2\right)^2 + \omega^2}} \tag{69}$$

The van Hove function and the intermediate scattering function have Gaussian shape in both $\mathbf{r}$ and $\mathbf{q}$, and the dynamic structure factor has the form of a *Lorentzian* in ω. Here the Gaussian approximation is exact. Free diffusion is the simplest dynamical process giving rise to *quasielastic* scattering (see Fig. 4). The half width at half maximum (HWHM) of the quasielastic line is given by

$$\boxed{\Gamma = Dq^2} \tag{70}$$

Examples for Lorentzian profiles are shown in Fig. 1.

Let us now compute the mean-square displacement associated with the model of free diffusion. For this purpose we write

$$W(t) = \int_V \int_V d^3R d^3R'\, P(\mathbf{R},t|\mathbf{R}',0) P_{eq}(\mathbf{R})(\mathbf{R}-\mathbf{R}')^2.$$

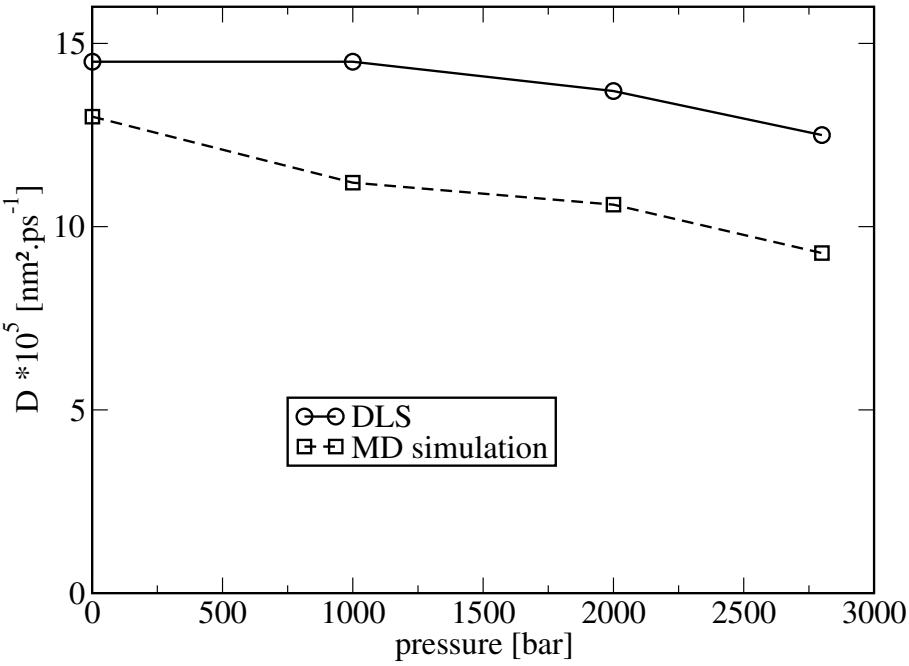

FIGURE 2. Diffusion coefficient for the CM of lysozyme from dynamic light scattering [**22**] and MD simulation [**21**].

Performing the trivial integration over $\mathbf{R}'$ and comparing the conditional probability density (65) with the van Hove correlation function (68) for free diffusion shows that

$$\boxed{W(t) = \int_V d^3r\, r^2 G(\mathbf{r},t) = 6Dt} \tag{71}$$

This is the well-known Einstein diffusion law for free diffusion. It shows that the molecules can move arbitrarily far from the origin. A consequence is that the $EISF$ for freely diffusing particles is zero. This follows immediately from its definition (30) which yields with (67) $EISF(\mathbf{q}) = \lim_{t\to\infty} I(\mathbf{q},t) = 0$.

A recent example for the application of the above scattering law to protein dynamics can be found in [**20**]. The diffusion constant for lysozyme is found to be $7.2 \pm 0.3 \cdot 10^{-7}\, cm^2/s$. Fig. 2 shows a recent calculation of the translational diffusion coefficient of lysozyme as a function of pressure obtained from MD simulation [**21**], as compared to results from dynamic light scattering (DLS) [**22**]. Although the statistics in the calculation of the diffusion constant from MD simulation is very poor (one single lysozyme molecule in a box water) the simulation results are in good agreement with DLS. The value of the diffusion constant measured by dynamic light scattering may be inserted into the Stokes-Einstein relation [**23**], assuming that the protein is sphere of radius

a,

$$\boxed{D = \frac{k_B T}{6\pi\eta a}} \tag{72}$$

In this expression η is the viscosity of the solvent, which is in practice water with $\eta = 1.002\, Pa \cdot s$ at room temperature ($1\, Pa = 1\, N/m^2$). Using the diffusion constant from dynamic light scattering [**22**], $D = 1.45\, 10^{-6} cm^2/s$, one finds $a = 1.47\, nm$. This is the radius of a lysozyme molecule if the latter is approximated by a sphere. This simple calculation is not necessarily a proof that the neutron scattering result is wrong. Apart from hydration shells, which influence the effective hydrodynamic radius of a protein, the diffusion constant is influenced by long-ranged electrostatic forces between the diffusing protein molecules, as well as by hydrodynamic interactions. It is probably not reasonable to assume that the hydration shells in the light and neutron scattering experiments are very different and so thick that they could double the diameter of the lysozyme molecule. At concentrations of 60-80 mg/ml, which correspond to the experimental situation, hydrodynamic interactions are not yet strong and the diffusion constant is predominantly influenced by intermolecular electrostatic forces which depend considerably on screening effects produced by the presence of dissociated salt in the solution. One should also keep in mind that DLS does not directly probe single particle diffusion [**24**]. All these points must be considered in detail in order to understand the difference of the diffusion constants observed by neutron scattering and DLS.

2.2. Rotational diffusion of molecules. Rotational diffusion is a more complicated process than the isotropic translational diffusion discussed above since the molecules are now described as rigid bodies and not as points. Let us for the moment consider one single atom which moves on the surface of a sphere due to the molecular rotation. The latter is decribed by a set of angles $\Omega = (\alpha, \beta, \gamma)$, which we define to be the Euler angles (see Fig. 3). The time evolution of position of the selected atom is then described by

$$\boxed{\mathbf{r}(t) = \mathbf{D}\Big(\Omega(t)\Big) \cdot \mathbf{r}^{(0)}} \tag{73}$$

where $\mathbf{D}$ is a rotation matrix which is parametrized by the selected set of angles, Ω. The vector $\mathbf{r}^{(0)}$ is the initial position. Due to the purely rotational motion we have

$$|\mathbf{r}(t)| = R = \text{const.} \tag{74}$$

We consider again free diffusion, which is here free *rotational, isotropic* diffusion. This model applies to a diluted solution of spherical particles. The corresponding differential equation for $P(\Omega, t|\Omega', 0)$ reads (see Appendix 4)

$$\boxed{\partial_t P = \gamma_r \left\{ \frac{\partial^2}{\partial\beta^2} + \cot\beta \frac{\partial}{\partial\beta} + \frac{1}{\sin^2\beta}\left(\frac{\partial^2}{\partial\alpha^2} + \frac{\partial^2}{\partial\gamma^2}\right) - 2\frac{\cot\beta}{\sin\beta}\frac{\partial^2}{\partial\alpha\partial\gamma}\right\} P} \tag{75}$$

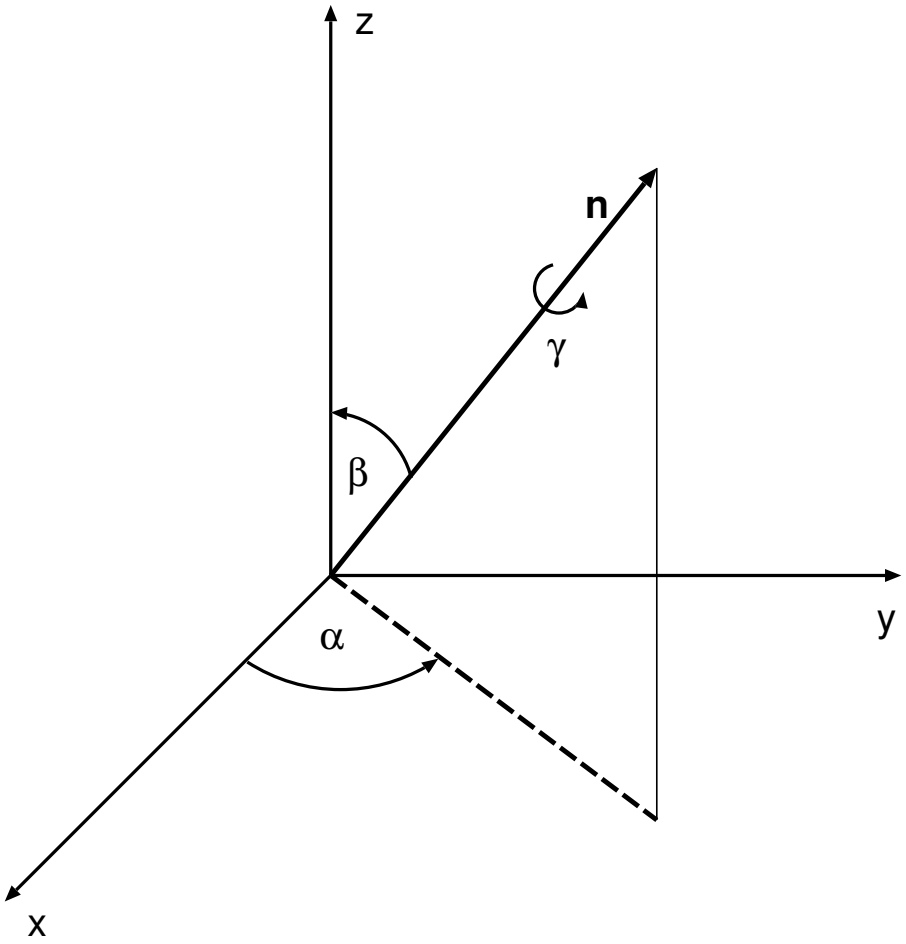

FIGURE 3. Definition of the Euler angles. Here **n** is a body-fixed unit vector whose orientation is specified by the angles α and β. The angle γ describes a rotation of the body about **n**.

Here γ_r is the *rotational diffusion constant* which has the dimension $1/s$ in SI units. The solution of (75) is derived in Appendix 4 and we give here directly the result,

$$P(\Omega,t|\Omega',0)=\sum_{l=0}^{\infty}\sum_{m,n=-l}^{+l}\frac{2l+1}{8\pi^2}\exp\Big(-\gamma_r l(l+1)t\Big)D^l_{mn}(\Omega)D^{l*}_{mn}(\Omega'). \tag{76}$$

where $D^l_{mn}(\Omega)$ are the Wigner rotation matrices [**25, 26**]. The equilibrium density is here

$$P_{eq}(\Omega)=\lim_{t\to\infty}P(\Omega,t|\Omega',0)=\frac{1}{8\pi^2}. \tag{77}$$

Inserting (76) into (60) yields the intermediate scattering function[2] (see Appendix 4)

$$I(\mathbf{q},t;R)=\sum_{l=0}^{\infty}(2l+1)j_l^2(qR)\exp\Big(-\Gamma_l t\Big). \tag{78}$$

where we have defined

$$\boxed{\Gamma_l = l(l+1)\gamma_r} \tag{79}$$

The parameters R indicates that the intermediate scattering function corresponds to a fixed radius. We assume now that the diffusing protein can be approximated by a sphere of radius a and that the distribution of hydrogen atoms in the protein is homogeneous. This is a reasonable assumption since hydrogen atoms are contained in all amino acids at approximately equal proportion. With this premise one can average expression (78) over a spherical shells ranging from $R=0$ to $R=a$. As a result

$$\boxed{I(\mathbf{q},t)=\sum_{l=0}^{\infty}(2l+1)A_l(qa)\exp(-\Gamma_l t)} \tag{80}$$

where the coefficients $A_l(qa)$ are given by

$$\boxed{A_l(qa)=\frac{3}{a^3}\int_0^a dR\,R^2 j_l^2(qR)} \tag{81}$$

The term with $l=0$ is the EISF shown in Fig. 4,

$$\boxed{EISF(qa)=A_0(qa)=\frac{3[2qa-\sin(2qa)]}{4q^3a^3}} \tag{82}$$

Fourier transform of expression (80) yields the dynamic structure factor for rotational diffusion

$$\boxed{S_{rot}(\mathbf{q},\omega)=A_0(qa)\delta(\omega)+\frac{1}{\pi}\sum_{l=1}^{\infty}(2l+1)A_l(qa)\,\frac{\Gamma_l}{\Gamma_l^2+\omega^2}} \tag{83}$$

To obtain an estimate for the rotational diffusion constant γ_r which determines the widths of the Lorentzians in the dynamic structure factor through the relation (79) one can use the analogue of the Stokes-Einstein (72) relation for rotational diffusion **[27]**

$$\boxed{\gamma_r=\frac{k_BT}{4\pi\eta a^3}} \tag{84}$$

Using lysozyme as an example, which has a radius of $a=1.45\,nm$, yields $\gamma_r=1.06\cdot10^8\,s^{-1}$ at $T=293K$, which corresponds to a rotational relaxation

[2]The $j_l(z)$ are the spherical Bessel functions.

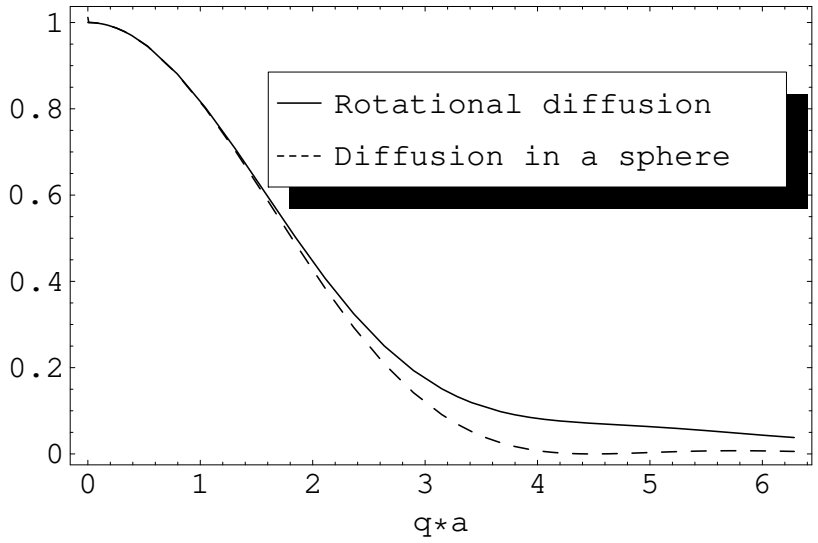

FIGURE 4. EISF for rotational diffusion of a spherical protein of radius a (solid line) and for diffusion of a point-like particle in a spherical cavity of radius a (dashed line).

time of $\tau_r = 9.4\,ns$, with $\tau_r \equiv \gamma_r^{-1}$. This example shows that rotational diffusion of whole proteins is a slow process on the neutron time scale. It is interesting to compare this time scale to the one of translational diffusion. If we use $D = 1.45 \cdot 10^{-6} cm^2/s$ **[22]** for the translational diffusion coefficient and $q = 1\,\text{Å}^{-1}$ we obtain $Dq^2 = 1.45 \cdot 10^{10}\,s^{-1}$ which corresponds to a relaxation time of $\tau = 69\,ps$. This shows that translational diffusion of proteins is considerably faster than rotational diffusion, except for higher orders of l. In the latter case the associated amplitudes $A_l(qa)$ are, however, small. We note also that the rotational EISF is small for momentum transfers of the order of $q \approx 1\,\text{Å}^{-1}$, which are characteristic for most spectrometers for quasielastic scattering experiments. In this case we have $qa \approx 20$ and $A_0(qa) \approx 0$. In such an experimental situation one may simply neglect the effect of rotational diffusion of whole proteins.

3. Internal motions

3.1. Diffusion inside a sphere. A simple model which can account for quasielastic scattering due to spatially confined motions is diffusion inside a sphere **[28]**. Applications to internal protein dynamics can be found in **[29]** and **[30]**. The dynamical variables are the spherical coordinates $\Omega \equiv \{r, \theta, \phi\}$. Here r is the distance of the diffusing hydrogen atom to the center of the sphere, and $\{\theta, \phi\}$ specify the direction of its position vector. The constraint for the motion is that $r \leq a$, where a is the radius of the sphere. The derivation

of the scattering law starts from the diffusion equation in the variables $\{r, \theta, \phi\}$ and proceeds along similar lines as for rotational diffusion. The calculation of $P(\Omega, t|\Omega', 0)$ is, however, more complicated and we give here only the results. For details we refer to **[28]**. As in the case of rotational diffusion, the intermediate scattering function has a multiexponential non-gaussian form:

$$\boxed{I(\mathbf{q}, t) = \sum_{l,n=0}^{\infty} (2l+1) A_n^l(q) \exp\left(-\Gamma_n^l t\right)} \tag{85}$$

Defining the numbers x_n^l through

$$l\, j_l(x_n^l) - x_n^l j_{l+1}(x_n^l) = 0 \qquad l > 0, \tag{86}$$

$$j_1(x_n^0) = 0 \qquad l = 0, \tag{87}$$

the functions $A_n^l(q)$ can be expressed as follows: For $\{l, n\} \neq 0, 0$ one has[3]

$$A_n^l(q) = \begin{cases} \frac{6(x_n^l)^2}{(x_n^l)^2 - l(l+1)} \left[\frac{qa\, j_{l+1}(qa) - l j_l(qa)}{(qa)^2 - (x_n^l)^2}\right]^2, & qa \neq x_n^l \\ \frac{3}{2} j_l^2(x_n^l) \frac{(x_n^l)^2 - l(l+1)}{(x_n^l)^2}, & qa = x_n^l. \end{cases} \tag{88}$$

In (85) $\Gamma_0^0 = 0$, and the term with $\{l, n\} = 0, 0$ thus yields the EISF (see fig. 4),

$$\boxed{EISF(\mathbf{q}) = A_0^0(q) = \left[\frac{3 j_1(qa)}{qa}\right]^2} \tag{89}$$

For $\{l, n\} \neq 0, 0$ the constants Γ_n^l are given by

$$\boxed{\Gamma_n^l = D\left(\frac{x_n^l}{a}\right)^2} \tag{90}$$

The relations (86) and (87) follow from boundary conditions for the radial part of $P(\Omega, t|\Omega', 0)$ and account for the condition that the diffusing particle must stay inside a sphere of a given radius.

It follows from (85) that the dynamic structure factor takes the form

$$\boxed{S(\mathbf{q}, \omega) = A_0^0(q)\delta(\omega) + \frac{1}{\pi} \sum_{l,n \neq \{0,0\}}^{\infty} (2l+1) A_n^l(q) \frac{\Gamma_n^l}{(\Gamma_n^l)^2 + \omega^2}} \tag{91}$$

[3] As in the model for rotational diffusion, the $j_l(z)$ are the spherical Bessel functions.

3.2. Langevin oscillator. A model which allows to describe different types of internal motions in a protein is the Langevin oscillator. Varying the friction constant produces vibrational motions as well as purely diffusional motion which give rise to quasielastic scattering. To keep the presentation simple we consider for the moment one-dimensional motion. In this case the dynamical variables are the deviation of the oscillating atom from its equilibrium position and the corresponding velocity, $\Omega \equiv \{x, v\}$. The interaction of a tagged atom with its environment is described by a harmonic force,

$$\boxed{F(x) = -M\omega_0^2 x} \tag{92}$$

which tends to keep the atom close to its equilibrium position. Harmonic oscillation of a particle in the presence of a random force representing collisions with neighbor particles is described by the stochastic equation of motion

$$\boxed{\frac{d^2x}{dt^2} + \gamma_0 \frac{dx}{dt} + \omega_0^2 x = \frac{1}{M} F_s} \tag{93}$$

where F_s is a stochastic force with the properties

$$\langle F_s(t) \rangle = 0, \qquad \langle F_s(t) F_s(t') \rangle = 2\gamma_0 M k_B T \delta(t - t'). \tag{94}$$

Eq. (93) is a generalization to Langevin's equation of motion for free diffusion **[31]**.

3.2.1. *Fokker-Planck equation.* In order to be able to compute the intermediate scattering function one needs the equation of motion for a conditional probability density. In our case we need to describe the evolution of this conditional probability in (x, v)-space in presence of a harmonic potential, $U(x) = \frac{1}{2} M\omega_0 x^2$. The corresponding equation of motion is the *Fokker-Planck equation* **[32, 33, 34]**

$$\boxed{\frac{\partial P}{\partial t} = A_{ij} \frac{\partial}{\partial \Omega_i} (\Omega_j P) + B_{ij} \frac{\partial^2 P}{\partial \Omega_i \partial \Omega_j}}$$

Here we have used $\Omega \equiv \{\Omega_1, \Omega_2\} \equiv \{x, v\}$ to keep the notation compact. The matrices $\mathbf{A} \equiv (A_{ij})$ and $\mathbf{B} \equiv (B_{ij})$ are called drift and fluctuation matrix, respectively, and are defined as

$$\mathbf{A} = \begin{pmatrix} 0 & -1 \\ \omega_0^2 & \gamma_0 \end{pmatrix}, \qquad \mathbf{B} = \begin{pmatrix} 0 & 0 \\ 0 & \frac{k_B T}{M} \gamma_0 \end{pmatrix}. \tag{95}$$

The conditional probability density $P(\Omega, t|\Omega', 0)$ is a Gaussian in the variables $\Omega_1 \equiv x$ and $\Omega_1 \equiv v$ **[33]**,

$$P(\Omega, t|\Omega', 0) = (2\pi)^{-1} \left(\det \boldsymbol{\sigma}(t)\right)^{-1/2} \exp\left(-\frac{1}{2} (\Omega_i - \langle \Omega_i(t) \rangle) [\boldsymbol{\sigma}^{-1}(t)]_{ij} (\Omega_j - \langle \Omega_j(t) \rangle) \right), \tag{96}$$

The center of the Gaussian is given by [4]

$$\langle \Omega_i(t) \rangle = G_{il}(t)\Omega'_l, \qquad \mathbf{G} = \exp(-\mathbf{A}t), \tag{97}$$

and its width by

$$\sigma_{ij}(t) = \langle [\Omega_i(t) - \langle \Omega_i(t) \rangle] [\Omega_j(t) - \langle \Omega_j(t) \rangle] \rangle = 2 \int_0^t d\tau \, G_{ik}(\tau) B_{kl} G_{jl}(\tau). \tag{98}$$

It follows from the above relations that $P(\Omega, 0|\Omega', 0) = \delta(\Omega - \Omega')$ and that

$$P_{eq}(x) = (2\pi)^{-1} \Big(\det \boldsymbol{\sigma}(\infty) \Big)^{-1/2} \exp \left(-\frac{1}{2} \Omega_i [\boldsymbol{\sigma}^{-1}(\infty)]_{ij} \Omega_j \right). \tag{99}$$

On account of (98) one finds that

$$\sigma_{ij}(\infty) = \langle \Omega_i \Omega_j \rangle, \qquad \boldsymbol{\sigma}(\infty) = \frac{k_B T}{M} \begin{pmatrix} \omega_0^{-2} & 0 \\ 0 & 1 \end{pmatrix}. \tag{100}$$

3.2.2. *Gaussian form of the intermediate scattering function.* Starting with the above prerequisites one can now proceed to compute the intermediate scattering function according to (60). We omit the calculation and refer to **[35]** for details[5]. The result for $I(q,t)$ is then

$$\boxed{I(q,t) = \exp \left(-\frac{q^2}{2} W_x(t) \right)} \tag{101}$$

where $W_x(t)$ is the mean-square displacement,

$$W_x(t) = \langle [x(t) - x(0)]^2 \rangle,$$

which was introduced in (48). It is well known that the MSD can be expressed in terms of the *velocity autocorrelation function* (VACF) **[16, 36]**. Defining the latter as

$$c_{vv}(t) := \langle v(t) v(0) \rangle, \tag{102}$$

one can write **[16]**

$$\boxed{W_x(t) = \langle [x(t) - x(0)]^2 \rangle = 2 \int_0^t d\tau \, (t - \tau) c_{vv}(\tau)} \tag{103}$$

This shows that the time and q-dependent intermediate scattering function $I(q,t)$ is entirely determined by $c_{vv}(t)$.

---

[4] Here and following summation over two identical indices is implied. This means that $a_i b_i \equiv \sum_i a_i b_i$, $a_{ik} b_{kj} \equiv \sum_k a_{ik} b_{kj}$ etc.

[5] In this reference the multidimensional case is treated.

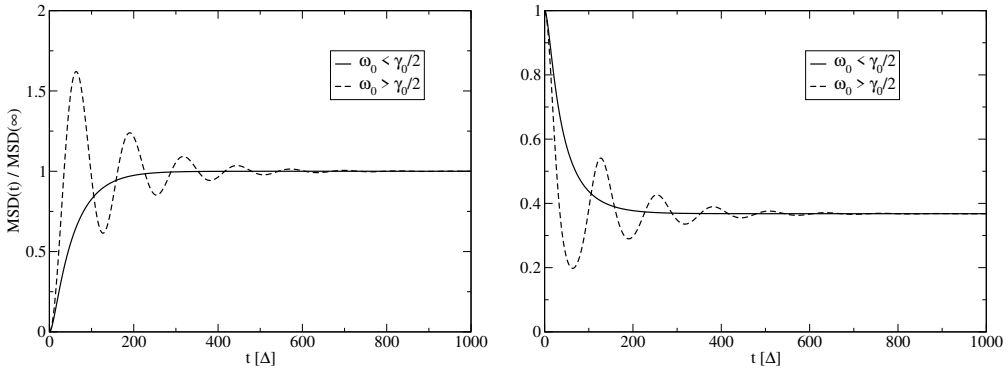

FIGURE 5. **Left:** MSD for the Langevin oscillator in the underdamped regime (dashed line) and in the overdamped regime (solid line). **Right:** Corresponding intermediate scattering function for a fixed value of q. The plateau value is the EISF.

3.2.3. *Velocity autocorrelation function.* From (93) one can derive a closed equation for $c_{vv}(t)$, using that the velocity of the Langevin oscillator is not correlated with the random force, $\langle v(0)F_s(t)\rangle = 0$. One obtains then

$$\frac{d^2c_{vv}}{dt^2} + \gamma_0\frac{dc_{vv}}{dt} + \omega_0^2 c_{vv} = 0. \tag{104}$$

One distinguishes two regimes[6]:

a) $\gamma_0/2 < \omega_0$ (underdamped motion)
b) $\gamma_0/2 > \omega_0$ (overdamped motion)

Depending on which case is considered, $c_{vv}(t)$ takes the form

$$c_{vv}(t) = \begin{cases} \frac{k_BT}{M}\exp\left(-\frac{\gamma_0 t}{2}\right)\left\{\cos\Omega t - \frac{\gamma_0}{2\Omega}\sin\Omega t\right\} & \gamma_0/2 < \omega_0, \\ \frac{k_BT}{M}\exp\left(-\frac{\gamma_0 t}{2}\right)\left\{\cosh|\Omega| t - \frac{\gamma_0}{2|\Omega|}\sinh|\Omega| t\right\} & \gamma_0/2 > \omega_0, \end{cases} \tag{105}$$

and its Fourier spectrum is given by (see Fig. 6)

$$g_{vv}(\omega) = \begin{cases} \frac{k_BT}{M}\frac{\gamma_0\omega^2}{\left(\frac{\gamma_0^2}{4}+(\omega-\Omega)^2\right)\left(\frac{\gamma_0^2}{4}+(\omega+\Omega)^2\right)} & \gamma_0/2 < \omega_0, \\ \frac{k_BT}{M}\frac{\gamma_0\omega^2}{\left(\omega^2+(\frac{\gamma_0}{2}-|\Omega|)^2\right)\left(\omega^2+(\frac{\gamma_0}{2}+|\Omega|)^2\right)} & \gamma_0/2 > \omega_0. \end{cases} \tag{106}$$

[6]All formulae to be derived in the following can be considered in the limiting case $\gamma_0/2 = \omega_0$.

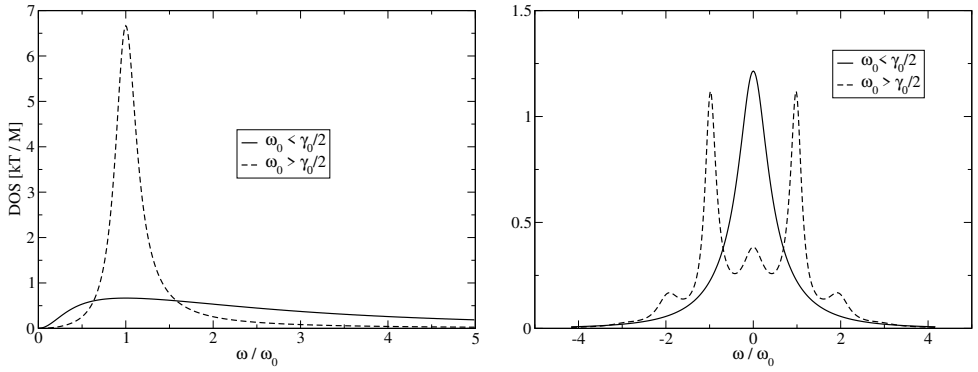

FIGURE 6. **Left:** $g_{vv}(\omega)$ in in arbitrary units for the under-damped regime (dashed line) and the over-damped regime (solid line). The frequency ω is shown for positive frequencies only. **Right:** Corresponding dynamic structure factors for a fixed value of q.

3.2.4. *Mean square displacement.* Using (103) we find that the MSD is given by

$$W_x(t) = \begin{cases} \frac{2k_BT}{M\omega_0^2}\left(1-\exp\left(-\frac{\gamma_0 t}{2}\right)\left\{\cos\Omega t + \frac{\gamma_0}{2\Omega}\sin\Omega t\right\}\right) & \gamma_0/2 < \omega_0, \\ \frac{2k_BT}{M\omega_0^2}\left(1-\exp\left(-\frac{\gamma_0 t}{2}\right)\left\{\cosh|\Omega| t + \frac{\gamma_0}{2|\Omega|}\sinh|\Omega| t\right\}\right) & \gamma_0/2 > \omega_0, \end{cases} \tag{107}$$

It follows that $W_x(t)$ tends to a plateau for $t \to \infty$ (see Fig. 5):

$$\boxed{\lim_{t\to\infty} W_x(t) = \frac{2k_BT}{M\omega_0^2}} \tag{108}$$

This follows from the fact that the motion is limited in space. In the limit $t \to \infty$ all cross-correlations between positions have decayed to zero and we have $W(\infty) = 2\langle x^2\rangle$ for motion which is confined in space. Therefore we can conclude from (108) that

$$\boxed{\langle x^2\rangle = \frac{k_BT}{M\omega_0^2}} \tag{109}$$

The above expression allows to extract an effective force constant, $K = M\omega_0^2$, from the scattering data [**37**].

3.2.5. *Analytical form of the intermediate scattering function.* We can now write down an analytical expression for the intermediate scattering function and the EISF. In the underdamped case we obtain

$$I(q,t) = \exp\left[-q^2\frac{k_BT}{M\omega_0^2}\left(1-\exp\left(-\frac{\gamma_0 t}{2}\right)\left\{\cos\Omega t + \frac{\gamma_0}{2\Omega}\sin\Omega t\right\}\right)\right] \tag{110}$$

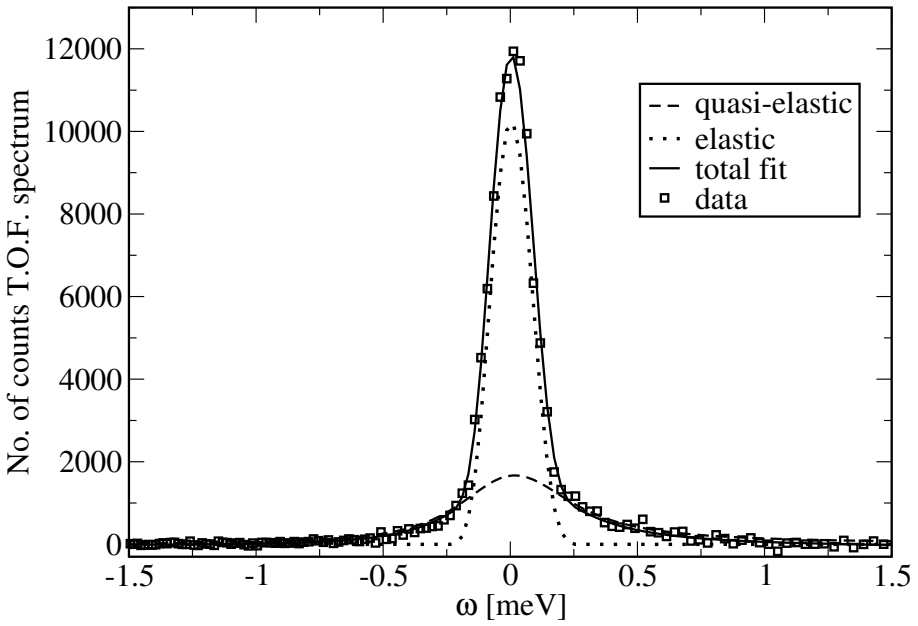

FIGURE 7. Fitted quasielastic spectrum of lysozyme in aqueous solution at room temperature **[21]** (compare sketch in Fig. 4). The data have been obtained with the time-of-flight spectrometer *Mibemol* at the Laboratoire Léon Brillouin in Saclay.

It follows that the EISF takes the simple form

$$\boxed{EISF(q) = \exp\left[-q^2 \frac{k_B T}{M\omega_0^2}\right]} \tag{111}$$

In the overdamped case $I(q,t)$ takes the form

$$I(q,t) = \exp\left[-q^2 \frac{k_B T}{M\omega_0^2}\left(1 - \exp\left(-\frac{\gamma_0 t}{2}\right)\left\{\cosh|\Omega|t + \frac{\gamma_0}{2|\Omega|}\sinh|\Omega|t\right\}\right)\right] \tag{112}$$

Note that the EISF does not depend on the friction constant, since it is a purely static average which is entirely determined by the harmonic potential function. The regime of Brownian motion is characterized by strongly overdamped motion, where $\gamma_0 \gg \omega_0$, and observation times $t \gg 1/\gamma_0$. In this case the intermediate scattering function reads **[35]**

$$I(q,t) = \exp\left[-q^2 \frac{k_B T}{M\omega_0^2}\left(1 - \exp\left(-\gamma_0^{-1}\omega_0^2 t\right)\right)\right]. \tag{113}$$

3.2.6. *Dynamic structure factor.* The dynamic structure factor for the Langevin oscillator cannot be obtained by an analytical formula. Fig. 6 shows a numerical calculation of $S'(q,\omega)$ for the underdamped regime (dashed line)

and the overdamped case (solid line). In the second case one sees only a single quasielastic line. If $\gamma_0 \to 0$ one obtains the spectrum of an harmonic oscillator without friction **[11]**. If $q^2\langle x^2\rangle \ll 1$ the intermediate scattering function may be expanded as

$$I(q,t) \approx 1 - \frac{q^2}{2} W_x(t). \tag{114}$$

If strongly overdamped motion is considered, $S'(q,\omega)$ takes the analytical form of a Lorentzian. This is seen from Eq. (113). Fitting the quasielastic spectrum for internal protein dynamics with a Lorentzian-shaped scattering profile yields, however, only a very rough estimate for the quasielastic line which is only valid for small energy transfers. As we will see later, protein dynamics is characterized by a large spectrum of relaxation rates and not by a single one. Fig. 7 shows an application of a Lorentzian fit to scattering data from lysozyme in solution **[21]** at $q_{el} = 1.5\,\text{Å}^{-1}$ (for elastic scattering). The instrumental resolution window is represented by a Gaussian. The data have been obtained with *Mibemol* spectrometer of the Laboratoire Leon Brillouin in Saclay. The experimental resolution was 48 μeV HWHM. Assuming a diffusion constant of $10^{-6}\,cm^2/s$ (see **[20]** and Fig. 2) as an order of magnitude yields a HWHM of $Dq^2 \approx 15\,\mu eV$, which is still below the resolution of the *Mibemol* spectrometer for the given experiment. This does, however, not mean that the quasielastic scattering profile is not influenced by global diffusion. The reason is that a Lorentz-profile decreases only $\propto \omega^{-2}$ for large frequencies.

CHAPTER 3

MD simulations and neutron scattering

As mentioned in the introduction, Molecular Dynamics (MD) simulations and neutron scattering experiments are probing the same length and time scales. Both methods can be considered as complementary experimental techniques. In this chapter it will be shown how MD simulations can be used to help understanding neutron scattering spectra.

1. The concept of MD simulations

The fundamental approximation of MD simulations is that the dynamics of the atoms in condensed matter systems can be described by Newton's laws of classical mechanics,

$$\boxed{m_\alpha \ddot{\mathbf{R}}_\alpha = -\frac{\partial U}{\partial \mathbf{R}_\alpha}} \tag{115}$$

Here each atom is represented by a mass point. The second approximation is that electronic degrees of freedom can be replaced by an *empirical force field*, $U(\{\mathbf{R}_\alpha\})$, in which electronic degrees of freedom are not considered explicitly. The force field $U(\{\mathbf{R}_\alpha\})$ depends on the positions of all atoms and describes the atomic interactions. During the last 20 years several force fields for biomolecular simulations have been developed (see e.g. references **[38, 39, 40, 41]**). The generic form is always similar:

$$\begin{aligned} U \;=\; & \sum_{\text{bonds}\,\alpha\beta} k_{\alpha\beta}\left(r_{\alpha\beta} - r^{(0)}_{\alpha\beta}\right)^2 \\ & + \sum_{\text{angles}\,\alpha\beta\gamma} k_{\alpha\beta\gamma}\left(\phi_{\alpha\beta\gamma} - \phi^{(0)}_{\alpha\beta\gamma}\right)^2 \\ & + \sum_{\text{dihedrals}\,\alpha\beta\gamma\delta} k_{\alpha\beta\gamma\delta}\cos\left(n_{\alpha\beta\gamma\delta}\theta_{\alpha\beta\gamma\delta} - \delta_{\alpha\beta\gamma\delta}\right) \\ & + \left.\begin{array}{l} \sum_{\text{pairs}\,\alpha\beta} 4\epsilon_{\alpha\beta}\left(\left[\frac{\sigma_{\alpha\beta}}{r}\right]^{12} - \left[\frac{\sigma_{\alpha\beta}}{r}\right]^{6}\right) \\ + \sum_{\text{pairs}\,\alpha\beta} \frac{q_\alpha q_\beta}{4\pi\epsilon_0 r_{\alpha\beta}} \end{array}\right\} \text{non-bonded} \end{aligned} \tag{116}$$

The first three lines contain the terms describing "bonded interactions" due to covalent bonds in a macromolecule (bond-stretching vibrations, bond-angle

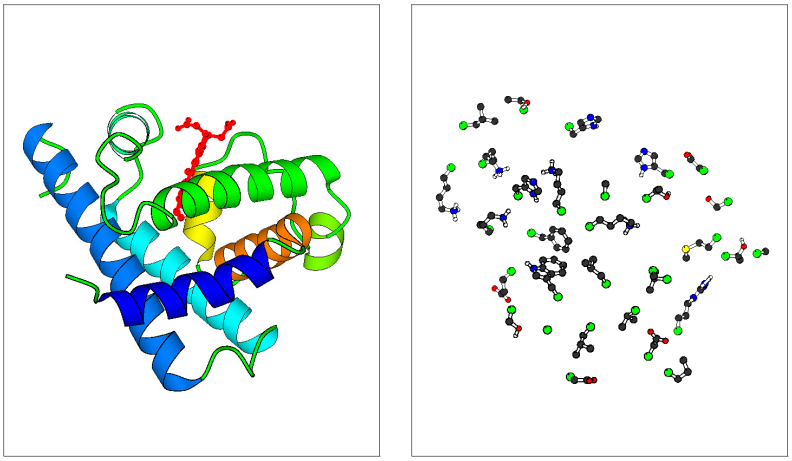

FIGURE 1. **Left** Protein backbone of myoglobin. **Right:** 31 selected side chains.

vibrations, and torsion angle dynamics). The last two lines describe "non-bonded interactions" due to excluded volume forces, dispersion forces, and electrostatic forces. The parameters are usually fitted to *ab initio* calculations of molecular fragments. The principle of an MD simulation is very simple. First Newton's equation of motion (115) is discretized. Using e.g. the Verlet algorithm **[42]** one obtains

$$\mathbf{R}_\alpha(n+1) = 2\mathbf{R}_\alpha(n) - \mathbf{R}_\alpha(n-1) + \frac{\Delta^2}{M}\frac{\partial U}{\partial \mathbf{R}_\alpha}, \tag{117}$$

where Δ is the integration time step which is of the order of one fs ($10^{-15}s$). In this integration scheme the velocities are obtained by the central difference

$$\dot{\mathbf{R}}_\alpha(n) \approx \frac{\mathbf{R}_\alpha(n+1) - \mathbf{R}_\alpha(n-1)}{2\Delta}. \tag{118}$$

In order to obtain a trajectory of one ns ($10^{-9}s$) one therefore has to perform 10^6 integration steps!

Once an MD trajectory has been generated, one can calculate correlation functions of dynamics variables A and B via

$$\langle A(0)B(m)\rangle = \frac{1}{N_t - m}\sum_{k=0}^{N_t-m-1} A(k)B(k+m). \tag{119}$$

Here N_t is the total number of configurations ("frames") in the stored trajectory. Note that static averages, such as the EISF, are obtained by putting $m = 0$ in (119).

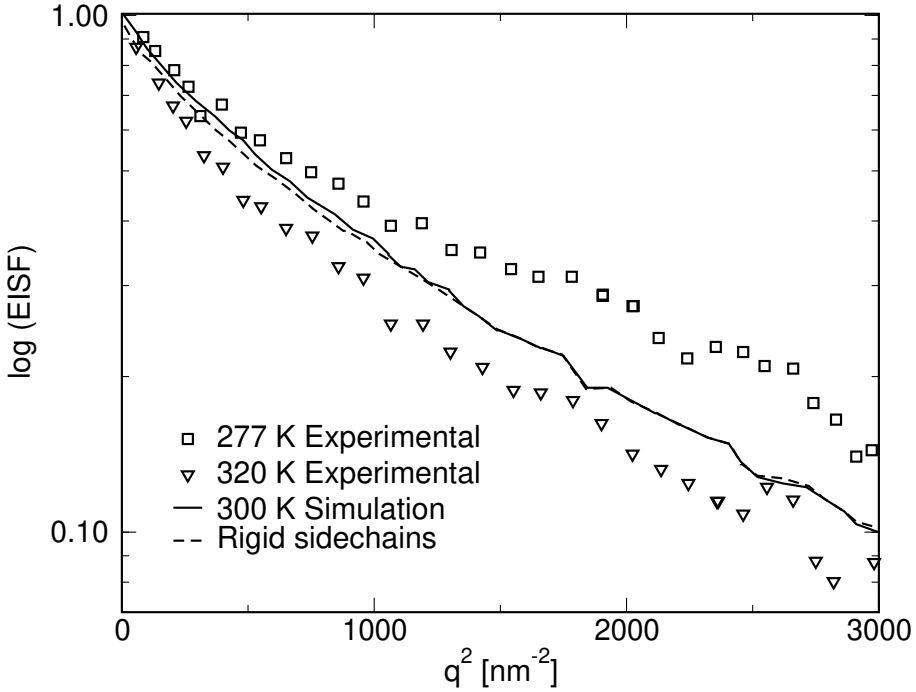

FIGURE 2. EISF of myoglobin from simulation [**43**] (solid line and dashed line) and experiment [**15**]. The solid line shows the result obtained from straightforward analysis of the MD trajectory and the dashed line has been obtained by filtering out internal motions of the protein side-chains.

2. Simple applications

2.1. Rigid-body motions in myoglobin. A simple application which gives an idea how MD simulations and neutron scattering experiments can be combined in a useful way has been published in [**43**]. The basic question addressed in this article is which type of motion contributes most to the quasielastic scattering spectrum of neutrons from myoglobin at room temperature – see again Fig. 5. The experimental data from DOSTER *et al.* [**15**] have been used in [**43**] to show that elastic and quasielastic neutron scattering from myoglobin (and quite probably from *all* globular proteins) is essentially produced by rigid-body motions of whole residues/side chains (see Fig. 1). Internal motions on the residue scale do almost not contribute to quasielastic and elastic neutron scattering (see Figs. 2 and 3). The rigid body trajectories have been produced by fitting to each side chain and each time frame a respective reference structure.

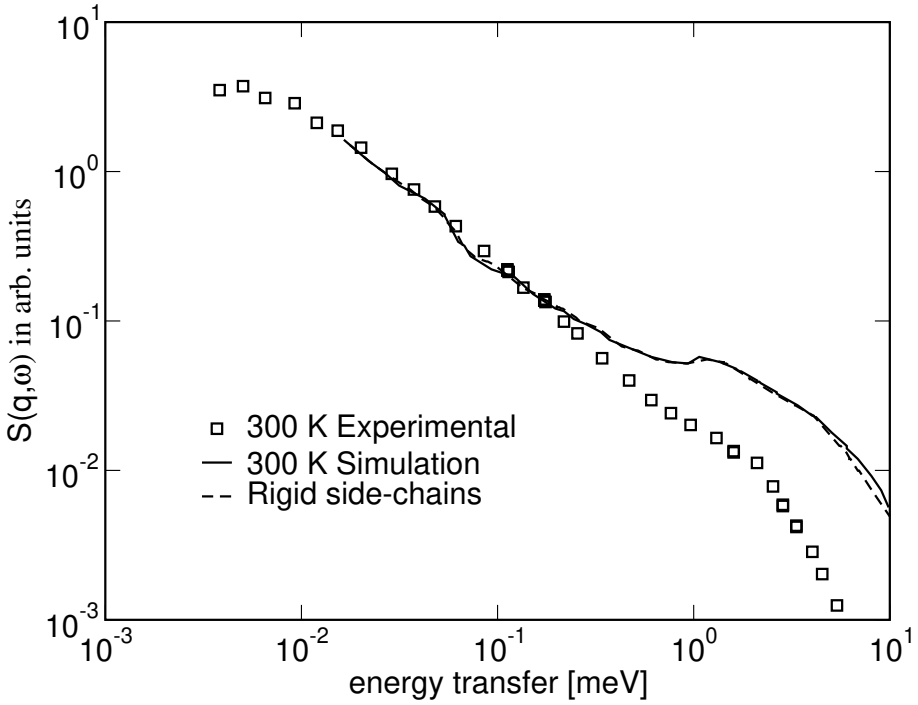

FIGURE 3. Results for the quasielastic spectrum correesponding to Fig. 2. In the experimental spectrum the vibrational contributions have been subtracted using a harmonic model [**15**]. This explains the disagreement between simulation and experiment for $\omega > 0.2\,meV$.

2.2. Testing the Gaussian approximation. It is obvious that the theoretical modeling of $I(q,t)$ can be considerably simplified if the GA is a reasonable approximation. Computer simulations allow to verify this in a very direct way. In contrast to "real" experiments, they allow quite easily to study arbitrary sub-ensembles and motion types of a given system. Let us consider lysozyme, which is a globular protein like myoglobin (see Fig. 4). To get an impression of the validity of the GA we consider first two sub-ensembles

- All (hydrogen) atoms
- The C_α atoms following only the backbone motion

For both ensembles we compute $I_H(q,t)$ and the corresponding GA. Figures 5 and 6 show the comparison for both ensembles. It is important to mention that the GA has here been applied to each atom *separately*, i.e. we average over the expressions (50) for all selected atoms. The results show the the GA gives almost perfect agreement for the C_α-atoms and is still very reasonable

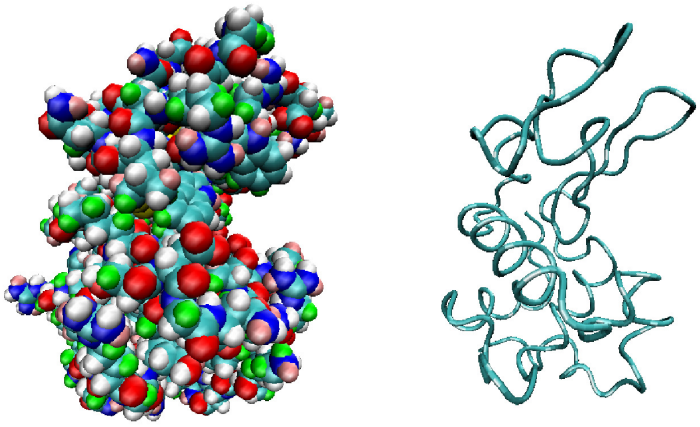

FIGURE 4. **Left:** The lysozyme molecule. Each atom is represented by a sphere with the corresponding van der Waals radius. **Right:** The backbone of the protein.

for the hydrogen atoms. According to (52) one would expect a straight line if $\ln(EISF)$ is plotted as a function of q^2.

Fig. 7 shows, however, that this is not the case, neither for the H-atoms, nor for the C_α-atoms, although the curve is clearly more linear in the latter case. To further discuss this point one needs to be aware that the non-linearity of $\ln(EISF)$ can have two reasons:

(1) Truly non-gaussian behavior, which can for example result from rotational motions of the side-chains.
(2) Apparent non-gaussian behavior due to motional heterogenity. Even if the GA is valid for each atom separately the EISF would not have the simple form (52) anymore. The reason is simply that a sum of two Gaussians (here in q) with different widths is not a Gaussian anymore.

Fig. 7 shows a decomposition of the EISF:

(1) The EISF from all atoms
(2) The EISF from the C_α-atoms
(3) The EISF from purely rotational side-chain motions. The latter have been obtained from the MD trajectory by rigid-body fits of reference structures for the side-chains (see **[43]** and references herein).
(4) The product of contributions 2) and 3).

The rotational side-chain motions give a strictly non-gaussian contribution. The fact that 1) and 4) are different shows that translational side-chain motions, which are given by the motions of the C_α atoms, and rotational side-chain motions are correlated.

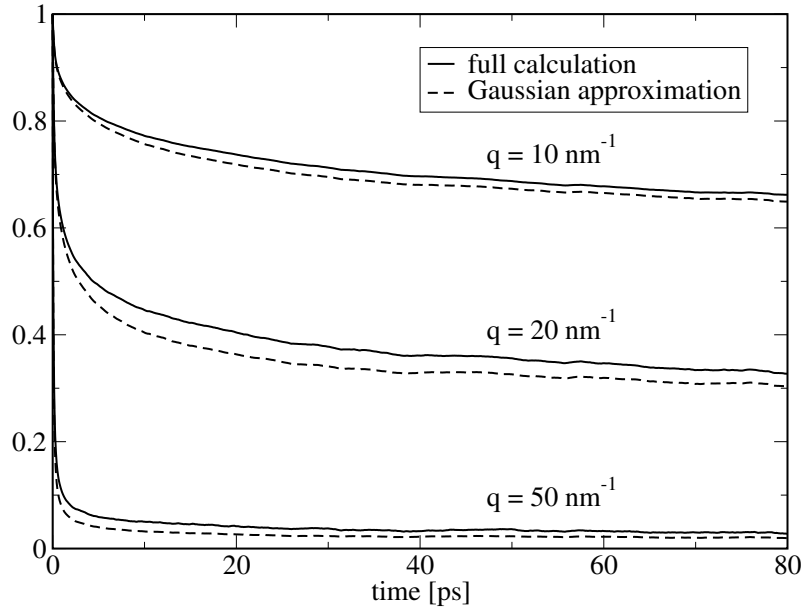

FIGURE 5. $I_H(q,t)$ for the hydrogen atoms in lysozyme by direct calculation (solid line) and by Gaussian approximation (dashed line).

3. Simulation-based modelling

In the following we discuss some applications of computer simulation which show how computer simulations can be used to develop dynamical models for protein dynamics.

3.1. "Non-gaussian" EISF from a gaussian model. The first application addresses the problem of motional heterogeneity which creates an apparent non-gaussian behaviour even if a gaussian model is valid for an individual atom. Fig. 9 shows the EISF of the C_α-atoms computed directly from MD data (solid line), as compared to the corresponding EISF obtained from an effective harmonic model allowing for motional heterogeneity (dashed line), and a fit of

$$EISF(q) = \exp(-q^2u^2) \tag{120}$$

to the EISF obtained from the effective harmonic model. Here u is a fit parameter which has been optimized for small values of q. The plot illustrates nicely that a non-linear EISF in a plot of $\ln(EISF)$ as a function of q^2 does not imply that the underlying dynamical model is really non-gaussian. It should be noticed that the EISF obtained from the effective harmonic model is much closer to the "real" EISF than to the fit (120).

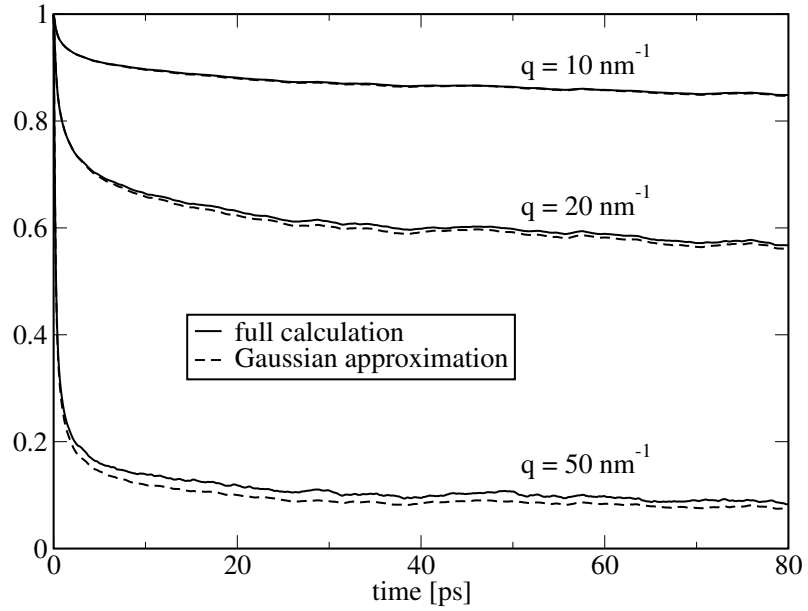

FIGURE 6. $I_H(q,t)$ for the C_α atoms in lysozyme by direct calculation (solid line) and by Gaussian approximation (dashed line).

To compute the EISF shown in Fig. 9 the model of coupled harmonic oscillators has been used. Each residue is represented by an "effective" C_α-atom whose mass is the total mass of the residue and whose scattering length is the average scattering length of all atoms in the residue (see Fig. 8). Such a model necessitates the construction of a "coarse-grained" force constant matrix from an all-atom force field used for protein simulations. This procesure is described in **[44]**. In generalization of (111) one obtains **[35]**

$$\boxed{EISF(\mathbf{q}) = \sum_{\alpha=1}^{N} w_\alpha \exp\left(-\sum_{k=1}^{3N} \frac{k_B T}{\tilde{\omega}_{\eta,j}^2}(\mathbf{q}^T \cdot \mathbf{d}_{j\alpha})^2\right)} \tag{121}$$

where the vectors $\mathbf{d}_{j\alpha}$ are three-dimensional subvectors of the eigenvectors (normal modes) $\mathbf{d}_j$ of the mass-weighted force constant matrix, and w_α are weights with $w_\alpha \propto b_{j,inc}^2$, where j runs over all atoms in residue α, and $\sum_{\alpha=1}^{N} w_\alpha = 1$. The force constant matrix is defined as

$$\boxed{\mathbf{K} = \mathbf{M}^{-1/2} \cdot \left(\frac{\partial^2 U}{\partial x_i \partial x_j}\right)\Big|_{\text{min.}} \cdot \mathbf{M}^{-1/2}} \tag{122}$$

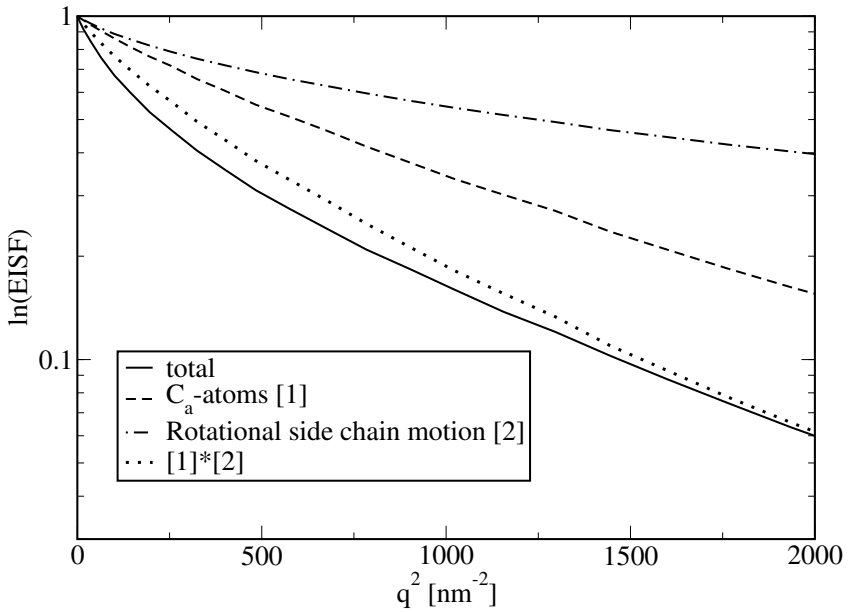

FIGURE 7. Decomposition of the EISF. Shown are the EISF for all atoms (solid line), the EISF for the C_α-atoms (long dashes), EISF from rigid side-chain motions (dashes and dots), and the product of the last two components.

where $\mathbf{M}$ is a diagonal mass matrix whose entries contain the total masses of the different residues. The normal modes are given by [1]

$$\boxed{\mathbf{K} \cdot \mathbf{d}_j = \tilde{\omega}_j^2 \mathbf{d}_j} \tag{123}$$

and the subvectors $\mathbf{d}_{j\alpha}$ are defined through $\mathbf{d}_{j\alpha} = (d_{j,3\alpha-2}, d_{j,3\alpha-1}, d_{j,3\alpha})^T$. The quantities $\tilde{\omega}_{\eta,j}$ appearing in (121) are *scaled* frequencies,

$$\boxed{\tilde{\omega}_{\eta,j} = \eta \tilde{\omega}_j}, \tag{124}$$

where $\eta < 1$ is a *global* scaling parameter which is chosen to fit the "real" EISF.

The frequencies $\tilde{\omega}_{\eta,j}$ are thus the characteristic frequencies of an *effective* harmonic potential. This idea is motivated by Frauenfelders view of a "rugged" multidimensional energy landscape of proteins **[18]** Fig. 10 shows this idea schematically. On a coarse-grained scale only one or a few minima exist. This envelope potential is perturbed by an enormous number of local subminima (conformational substates). At sufficiently high temperatures the system explores the full envelope potential. In our model **[44]** we make the approximation that the envelope potential has just one minimum, describing the

[1] The $\tilde{\omega}_j^2$ have the dimension of a force constant, i.e. kg/s^2 in SI units.

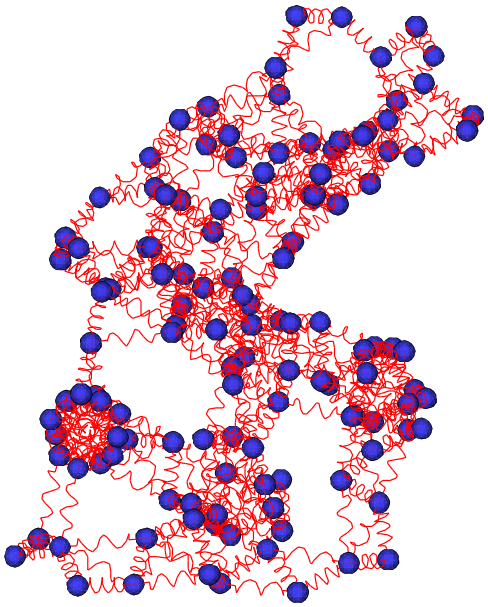

FIGURE 8. Coarse-grained harmonic model for lysozyme. Each residue is represented by an "effective C_α-atom".

native state of the protein, and that this global potential has a parabolic form. The second approximation is that this multidimensional parabola can be obtained from a normal mode expansion of one of the subminima, just scaling *all* eigenfrequencies to smaller values. This is equivalent to saying that the local minima and the minimum of the envelope potential are all similar in shape. Within this model above the glass transition temperature a protein would still move in an harmonic potential, which has just a smaller curvature. Going back to Figs. 7 and 8 shows that the evolution of the mean square fluctuations of myoglobin and bacteriorhodopsin in a purple membrane is consistent with this model. In the hydrated membrane the BR protein undergoes a dynamic transition and the mean square fluctuation of the hydrogen atoms increases still linearly, but with a steeper slope than below the transition temperature.

4. Brownian modes and multi-scale relaxation

The simplest way to extend the above model to account for dynamic properties is to introduce the notion of friction, accounting for frequent collisions between residues due to the "rugged" protein energy landscape [**44**]. Such a model should not be used on an atomic scale, where rapid side-chain motions contribute a non-gaussian, truly anharmonic component to protein dynamics (see Fig. 7). The motion of the residues in the envelope potential is described by strongly overdamped, purely diffusional motion. We recall that in the simplest case of one-dimensional motion of one single oscillator the intermediate

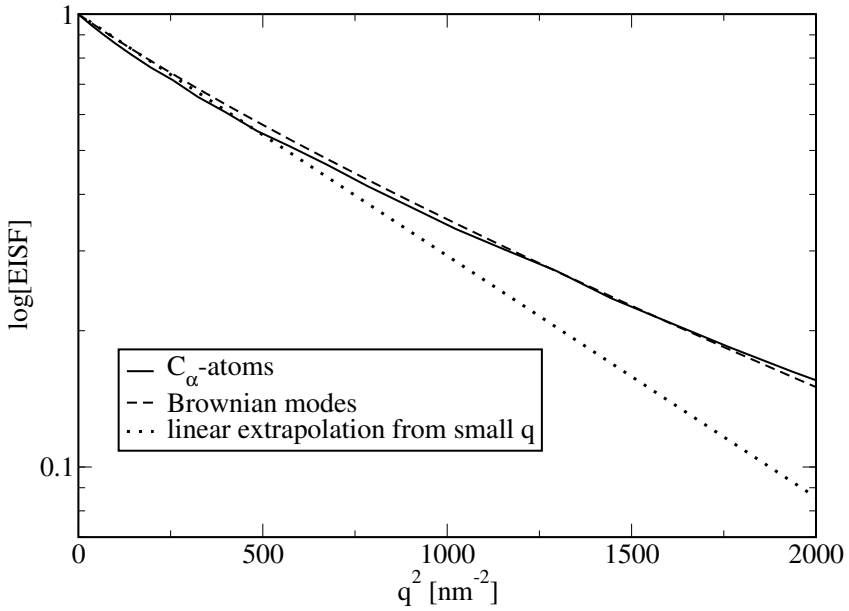

FIGURE 9. EISF for the C_α atoms from MD simulation (solid line), the corresponding EISF from an effective harmonic model with motional heterogeneity (dashed line), and an idealized EISF of the form $EISF = \exp(-q^2u^2)$ which has been fitted to the dashed curve for small values of q (see explanations in the text).

scattering function is given by expression (113). In case of coupled oscillators one obtains **[35]**

$$I_{BD}(\mathbf{q},t) = \sum_{\alpha=1}^{N} w_\alpha \exp\left[-\sum_{k=1}^{3N}\left(\frac{k_BT}{\hbar\omega_j^2}(\mathbf{q}^T\cdot\mathbf{d}_{j\alpha})^2 - \exp(-\lambda_k t)y_{\alpha\alpha}^{(k)}(\mathbf{q})\right)\right], \qquad (125)$$

where the weights w_α are defined as in (121). The quantities $y_{\alpha\alpha}^{(k)}(\mathbf{q})$ are quadratic forms in $\mathbf{q}$,

$$y_{\alpha\alpha}^{(k)}(\mathbf{q}) = k_BT\frac{(\mathbf{q}^T\cdot\mathbf{u}_{k\alpha})^2}{\mathbf{u}_k^T\cdot\mathbf{K}\cdot\mathbf{u}_k}. \qquad (126)$$

Here the vectors $\mathbf{u}_k$ are the *Brownian modes*, which are defined through

$$\boxed{\boldsymbol{\gamma}^{-1}\mathbf{K}\cdot\mathbf{u}_k = \lambda_k\mathbf{u}_k} \qquad (127)$$

where $\boldsymbol{\gamma}$ is a positive definite mass-weighted *friction matrix*. As for the vectors $\mathbf{d}_{j\alpha}$, one has here $\mathbf{u}_{j\alpha} = (u_{j,3\alpha-2}, u_{j,3\alpha-1}, u_{j,3\alpha})^T$. In **[44]** the friction matrix was assumed diagonal.

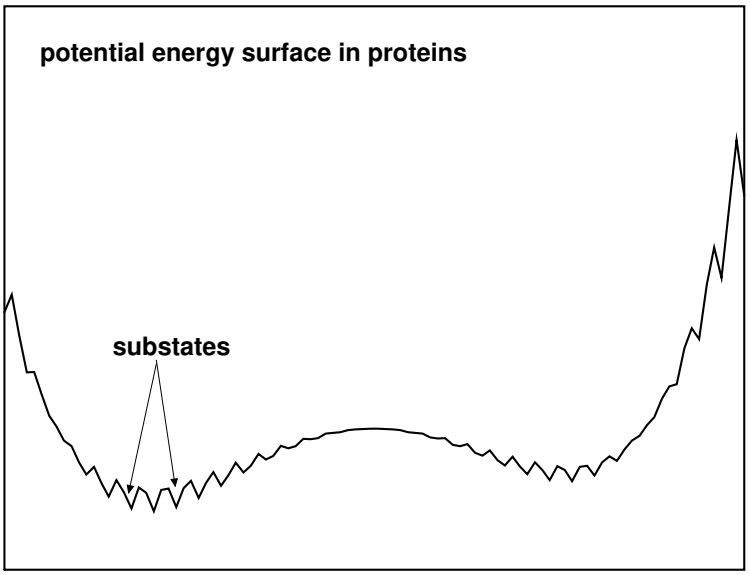

FIGURE 10. Frauenfelder's schematic view of a "protein energy landscape". See text for more explanations.

Eq. (125) shows that the dynamical behavior of $I_{BD}(\mathbf{q},t)$ is determined by a *spectrum of relaxation times*,

$$\boxed{\tau_k = \lambda_k^{-1}} \tag{128}$$

The above considerations show that multi-scale relaxation processes can be described by coupling harmonic degrees of freedom in presence of friction. Fig. 11 shows a comparison of the incoherent scattering function of C-phycocyanin on the residue level as computed from MD simulation and from Brownian modes [**44**]. The very fast drop-off at $t = 0$ has been modeled by an independent vibrational contribution, writing

$$I_{C_\alpha}(\mathbf{q},t) = I_{BD}(\mathbf{q},t) I_{vib}(\mathbf{q},t). \tag{129}$$

Here $I_{vib}(\mathbf{q},t)$ is computed using a standard normal mode calculation on the basis of an effective force constant matrix for the coarse-grained description on the residue level. It describes fast vibrations in local minima, and a small damping constant accounts for a finite life time of these oscillations.

4.1. Memory functions. A completely different approach to multi-scale relaxation is to describe the time evolution of intermediate scattering function

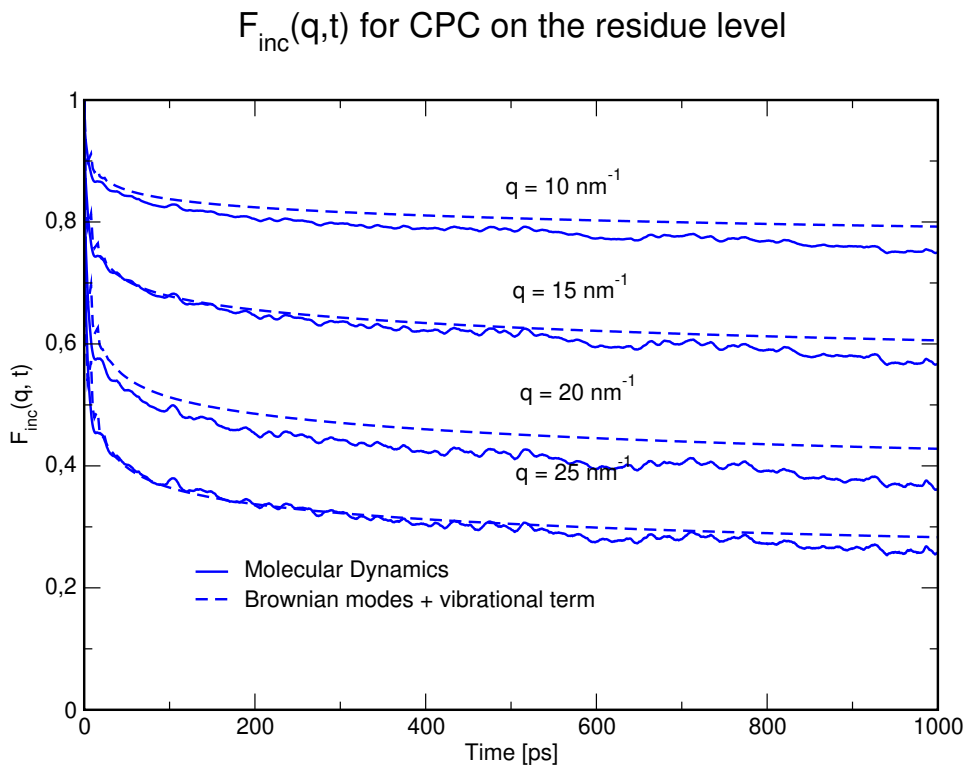

FIGURE 11. The incoherent scattering function for C-phycocyanin on the residue level. Each residue is represented by a point located at the C_α-position on the backbone. The figure shows a comparison of the direct calculation from MD simulation and the corresponding result obtained from Brownian modes and normal modes.

by a so-called memory function equation. The concept of memory functions has been introduced by Robert Zwanzig in the 1960's to describe the dynamics of liquids on a rigorous theoretical basis **[45, 16]**. The concept is, however, quite general. It applies to the time correlation function of any dynamical variable of a Hamiltonian system. The result is a formal equation of motion for the correlation function. For the intermediate scattering function one would write

$$\boxed{\partial_t I(\mathbf{q},t) = -\int_0^t d\tau\, \xi(\mathbf{q},t-\tau) I(\mathbf{q},\tau)} \tag{130}$$

Here $\xi(\mathbf{q},t)$ is the *memory function*. It can be interpreted as a generalized friction coefficient. In case of confined motion the memory function equation (130) is applied to $I'(\mathbf{q},t) = I(\mathbf{q},t) - EISF(\mathbf{q})$.

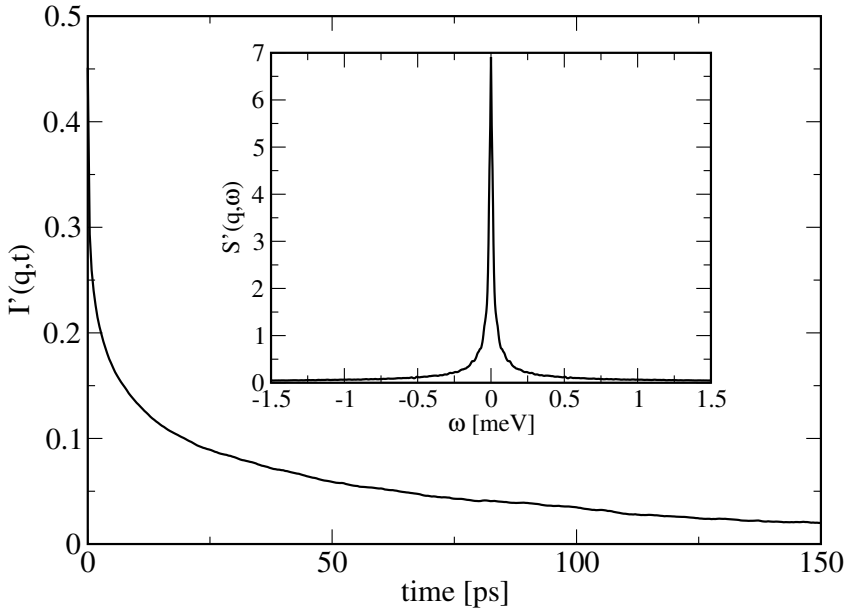

FIGURE 12. Simulated incoherent intermediate scattering function, $I'(\mathbf{q},t)$, of lysozyme, averaged over 30 momentum transfer vectors with $q_{el} = 1.5\,\text{Å}^{-1}$. The corresponding dynamic structure factor, $S'(\mathbf{q},\omega)$, is shown in the inset.

If we set[2]

$$\boxed{\xi(\mathbf{q},t) = Dq^2\delta(t)} \tag{131}$$

equation (130) reduces to a simple differential equation

$$\partial_t I(\mathbf{q},t) = -Dq^2 I(\mathbf{q},t). \tag{132}$$

The solution is a simple exponential,

$$\boxed{I(\mathbf{q},t) = \exp(-Dq^2 t)} \tag{133}$$

which is known to describe free diffusion (see Eq. (67)).

These simple considerations show that random motion, such as free diffusion, is characterised by short-ranged memory functions and corresponding simple exponential correlation functions. Such models are adequate to describe global protein dynamics, such as translational motion of whole protein molecules, but they are inadequate to describe internal protein dynamics. "Short-ranged" means here short-ranged with respect to the characteristic time scale of the corresponding correlation function, and not short-ranged on an absolute time scale.

[2] $\delta(t)$ is the Dirac delta distribution defined in Eq. (33). Its essential properties are $\int_{-\infty}^{+\infty} dx\,\delta(x) = 1$ and $\int_{-\infty}^{+\infty} dy\,\delta(x-y)f(y) = f(x)$.

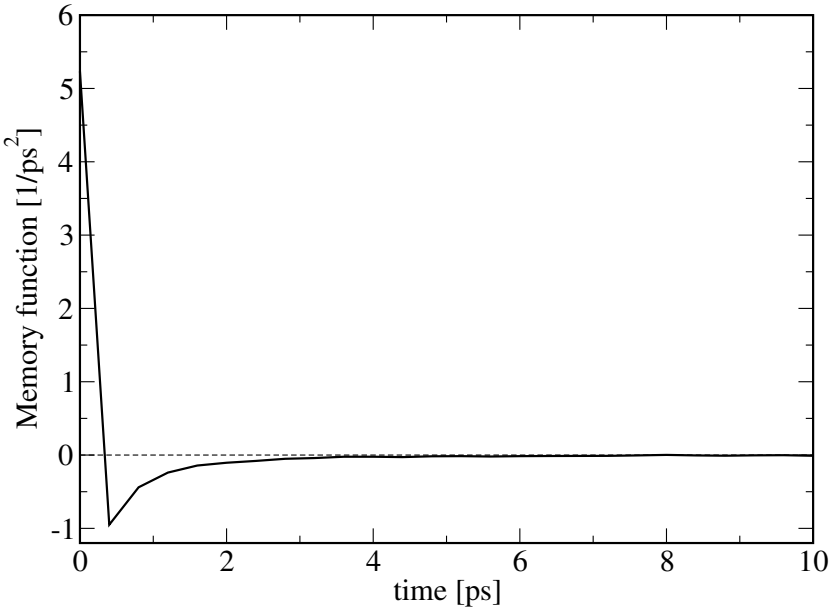

FIGURE 13. Memory function corresponding to $I'(\mathbf{q},t)$ depicted in Fig. 12.

It is well known that internal protein dynamics exhibits an enormous range of time scales, ranging from sub-picoseconds to seconds. Due to the high atomic density within a protein all these motions are coupled. This means that there is no characteristic time scale for $I'(\mathbf{q},t)$. The corresponding memory function is "long-ranged", in the sense that is decays not exponentially, but with a power law in time. Although the accessible time scale of MD simulations is limited to the ns range, they can show a fingerprint of long-ranged memory functions **[46]**. Fig. 12 shows the simulated intermediate function, $I'(\mathbf{q},t)$, of lysozyme and the corresponding dynamic structure factor $S'(\mathbf{q},\omega)$. The memory function is shown in in Fig. 13. All functions have been computed using an autoregressive model for the underlying time series $\exp[i\mathbf{q}^T \cdot \mathbf{R}_\alpha(t)]$ for each atom **[9, 47]** and each q-vector. Fig. 13 shows that $\xi(\mathbf{q},t)$ has an algebraic long-time tail of the form

$$\boxed{\xi(\mathbf{q},t) \propto (\beta-1)\left(\frac{t}{\tau}\right)^{\beta-2}} \tag{134}$$

where $\tau > 0$ and $0 < \beta < 1$. The form (134) is characteristic for stochastic processes with long-time memory **[48, 49]**. We note that the short-time behavior of $\xi(\mathbf{q},t)$ is not well resolved since a coarse-grained autoregressive model with a sampling interval of $\Delta t = 0.4\,ps$ has been used. The fact that internal protein dynamics is chartacterised by multi-timescale relaxation, and can thus not be described by exponential correlation functions, is illustrated in fig. 14.

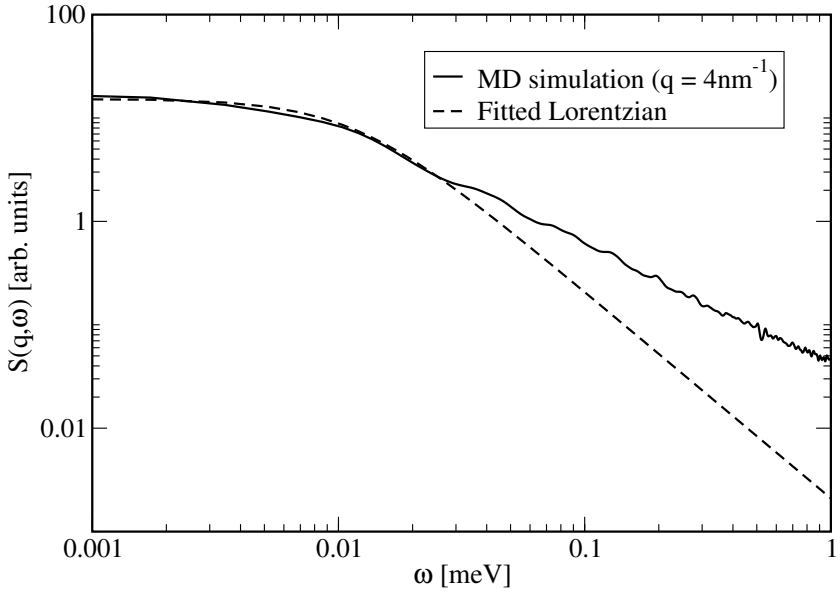

FIGURE 14. Simulated incoherent dynamic structure factor for lysozyme in solution at $q = 0.4\,\text{Å}^{-1}$ (solid line) and fit by a Lorenzian (dashed line).

The latter shows a log-log plot of the incoherent dynamic structure factor for lysozyme in solution, which has been obtained from MD simulation in the same way as the functions shown in fig. 12. For comparison a least squares fit of a Lorentzian profile to the data shown. Clearly the simulation data cannot be described by such a function. In this context we refer to fig. 7 in which a Lorentzian has been used to fit the quasielastic line. As already mentioned, the fit is only good for smaller energy transfers, which is less visible since the data are not shown in a log-log representation. We remark that the simulation data are well described by the model of fractional Brownian dynamics **[49]** to which a memory function of the form (134). The associated dynamic structure factor has the form **[46]** (the q-dependence is dropped)

$$\boxed{S_{fBD}(\omega) = \frac{2\tau \sin(\beta\pi/2)}{|\omega\tau|\,(|\omega\tau|^{\beta} + 2\cos(\beta\pi/2) + |\omega\tau|^{-\beta})}, \quad 0 < \beta \leq 1} \tag{135}$$

where τ and β are the parameters of the model. In the above form $S_{fBD}(\omega)$ is normalised to one. One recognises that $S_{fBD}(\omega) \longrightarrow 2\tau/(1 + [\omega\tau]^2)$ for $\beta \to 1$. In this case one retrieves exponential relaxation.

Let us now see how the internal protein dynamics is reflected in an experimental quasi-elastic spectrum. For this purpose we use the quasielastic scattering data for lysozyme in solution which have already been shown in

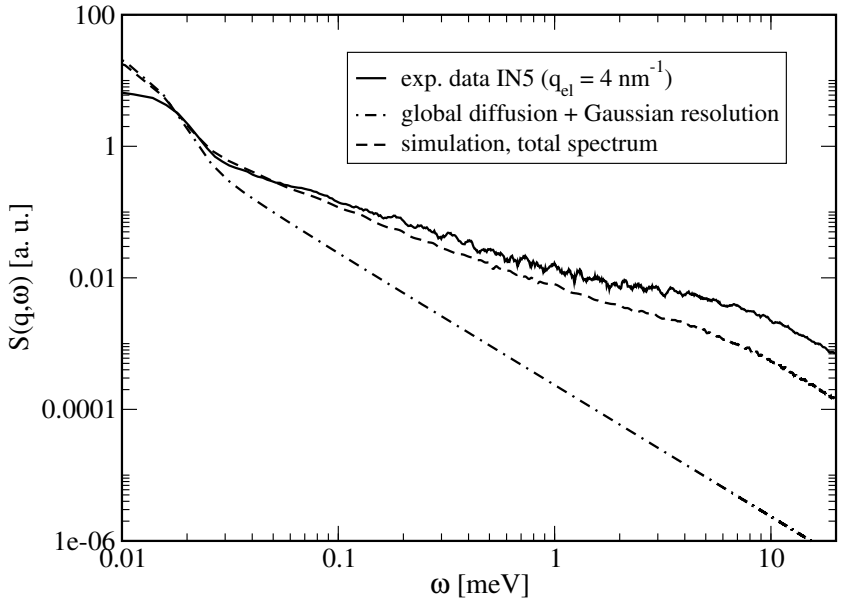

FIGURE 15. Experimental data from lysozyme in solution (solid line) confronted to the corresponding simulated spectrum (dashed line) and a theoretical scattering law for resolution broadened diffusion of whole molecules (dot-dashed) line. The experimental data are the same as in Fig. 9 of Chapter 1 for $q_{el} = 4\,nm^{-1}$ ($q_{el} = 0.4\,\text{Å}^{-1}$).

Fig. 9 of Chapter 1 (see refs. [**19, 21**]). The solid line shows the experimental spectrum for $q_{el} = 0.4\,\text{Å}^{-1}$. For comparison with the experimental data the simulated spectrum (dashed line) has been treated using expression (56). The scattering law for global diffusion was modelled by free diffusion with a diffusion coefficient of $7.2 \cdot 10^{-7}\,cm^2/s$ which is the valued measured in [**20**]. The resulting scattering law was finally convoluted with a Gaussian resolution function with a width of $\sigma = 7\,\mu eV$, which corresponds to the resolution of the IN5 spectrometer at the Institut Laue Langevin. The plot illustrates nicely that above about $0.2\,\text{e}V$ really *internal* protein dynamics is seen, which is not completely masked by the global diffusion of the lysozyme molecules. It should be noted that for higher energy transfers the comparison between experimental and simulated could be even more perfect if one takes into account that the simulation data are obtained at constant q, whereas the experimental data are obtained at constant scattering angle θ, corresponding to $q_{el}(\theta) = 4\,\text{Å}^{-1}$. Multiple scattering effects, which are not accounted for, may also play a role.

CHAPTER 4

Appendix

$I(\mathbf{q}, t)$ for rotational diffusion

To derive the differential equation for $P(\Omega, t|\Omega', t')$ we proceed as follows. As for translational diffusion, we can assume that $P(\Omega, t|\Omega', t')$ depends only on time differences $t - t'$, since equilibrium is assumed. We can then put $t' = 0$. One starts from a multidimensional diffusion equation like (63), where $\mathbf{r} = (\mathbf{r}_1^T, \ldots, \mathbf{r}_N^T)^T$ now comprises *all* particle positions. The next step is to make a coordinate transformation from the coordinates $\mathbf{r}$ to the generalized coordinates $\mathbf{\Omega}$, using (73). Using the tools of Riemannian differential geometry, one can derive a diffusion equation for an *arbitrary* set of generalized coordinates, $\Omega = (\Omega^1, \ldots, \Omega^f)^1$ **[50]**. Introducing the Jacobian $\mathbf{J} = \left(\frac{\partial r^i}{\partial \Omega^j}\right)$ and the metric matrix $\mathbf{g} \equiv (g_{ik}) = \mathbf{J}^T \cdot \mathbf{J}$, we obtain

$$\partial_t P = \frac{D}{\sqrt{g}} \frac{\partial}{\partial \Omega^i} \left\{ \sqrt{g} g^{ik} \frac{\partial}{\partial \Omega^k} \right\} P. \tag{136}$$

Here $g = \det(\mathbf{g})$, $(g^{ik}) \equiv \mathbf{g}^{-1}$, and summation over pairwise upper and lower indices is implicitly assumed. If the generalized coordinates are Euler angles, i.e. $\Omega \equiv (\alpha, \beta, \gamma)^T$, and the molecule under consideration is spherically symmetric, (136) takes the form

$$\frac{\partial P}{\partial t} = \gamma_r \hat{\mathcal{L}}_\Omega P \tag{137}$$

where $\hat{\mathcal{L}}_\Omega$ is the differential operator

$$\hat{\mathcal{L}}_\Omega = \frac{\partial^2}{\partial \beta^2} + \cot\beta \frac{\partial}{\partial \beta} + \frac{1}{\sin^2\beta} \left(\frac{\partial^2}{\partial \alpha^2} + \frac{\partial^2}{\partial \gamma^2} \right) - 2 \frac{\cot\beta}{\sin\beta} \frac{\partial^2}{\partial \alpha \partial \gamma}, \tag{138}$$

and γ_r is the *rotational diffusion constant*. It has the dimension $1/s$ in SI units.

Eq. (137) has to be solved with the initial condition

$$P(\Omega, 0|\Omega', 0) = \delta(\Omega - \Omega'), \tag{139}$$

[1] In the literature on differential geometry the generalized variables are indexed as Ω^i and not as Ω_i.

where $\delta(\Omega-\Omega')$ is the Dirac δ distribution in angular space. Any well-behaved function, $f(\Omega)$, in angular space can be developed in the basis of Wigner functions, $D^l_{mn}(\Omega)$ **[25, 26]**. The latter are eigenfunctions of $\hat{\mathcal{L}}_\Omega$,

$$\hat{\mathcal{L}}_\Omega D^l_{mn}(\Omega) = -l(l+1)D^l_{mn}(\Omega), \tag{140}$$

and fulfill the orthogonality relation

$$\int d\Omega\, D^l_{mn}(\Omega) D^{l'*}_{m'n'}(\Omega) = \frac{8\pi^2}{2l+1}\delta_{ll'}\delta_{mm'}\delta_{nn'}, \tag{141}$$

where $d\Omega = \sin\beta\, d\alpha\, d\beta\, d\gamma$. The angular δ-function can be written in the form

$$\delta(\Omega-\Omega') = \sum_{l=0}^{\infty}\sum_{m,n=-l}^{+l}\frac{2l+1}{8\pi^2}D^l_{mn}(\Omega)D^{l\,*}_{mn}(\Omega'). \tag{142}$$

Using the above definitions, $P(\Omega,t|\Omega',0)$ may be expanded as

$$P(\Omega,t|\Omega',0) = \sum_{l=0}^{\infty}\sum_{m,n=-l}^{l}\sum_{m',n'=-l'}^{l'} p^l_{mn}(t)q^{l'}_{m'n'}D^l_{mn}(\Omega)D^{l',*}_{m'n'}(\Omega'), \tag{143}$$

where $p^l_{mn}(t)$ are functions of time and $q^{l'}_{m'n'}$ are constants. To satisfy the initial condition (139) we have the constraint

$$p^l_{mn}(0)q^{l'}_{m'n'} = \frac{2l+1}{8\pi^2}\delta_{ll'}\delta_{mm'}\delta_{nn'}. \tag{144}$$

If (143) is inserted into the rotational diffusion equation (137), one obtains a simple differential equation for $p^l_{mn}(t)$ by using the eigenvalue equation (140),

$$\frac{\partial p^l_{mn}}{\partial t} = -\gamma_r l(l+1)p^l_{mn}. \tag{145}$$

The solutions are simple exponentials which depend only on l:

$$p^l_{mn}(t) = p^l_{mn}(0)\exp\Big(-\gamma_r l(l+1)t\Big). \tag{146}$$

This form for $p^l_{mn}(t)$ may now be inserted together with condition (144) into the general form (143) for the conditional probability. One obtains

$$P(\Omega,t|\Omega',0) = \sum_{l=0}^{\infty}\sum_{m,n=-l}^{+l}\frac{2l+1}{8\pi^2}\exp\Big(-\gamma_r l(l+1)t\Big)D^l_{mn}(\Omega)D^{l\,*}_{mn}(\Omega'). \tag{147}$$

As the translational transition probability density $P(\mathbf{R},t|\mathbf{R}',0)$ depends only on position differences, $P(\Omega,t|\Omega',0)$ depends only on the *relative* orientation Ω_r relating Ω' and Ω. For a rotation represented by a hermitean rotation matrix $\mathbf{D}(\Omega)$, such as a Wigner matrix, one can write $\mathbf{D}(\Omega) = \mathbf{D}(\Omega_r)\cdot\mathbf{D}(\Omega')$, or,

equivalently, $\mathbf{D}(\Omega_r) = \mathbf{D}(\Omega) \cdot \mathbf{D}^{\dagger}(\Omega')$, where † denotes the hermitean conjugate (conjugate complex of the transposed matrix). We thus have in components

$$D^l_{mk}(\Omega_r) = \sum_k D^l_{mn}(\Omega) D^{l*}_{kn}(\Omega') \tag{148}$$

which relates the corresponding Wigner matrices. On account of this expression one may thus write

$$P(\Omega_r, t|0,0) = \sum_{l=0}^{\infty} \sum_{m=-l}^{+<l} \frac{2l+1}{8\pi^2} \exp\Big(-\gamma_r l(l+1)t\Big) D^l_{mm}(\Omega_r). \tag{149}$$

In the case of rotational motion the van Hove correlation function is not of much interest, and we calculate only the intermediate scattering function. Since the observed intermediate scattering function for a protein solution does not depend on the direction of $\mathbf{q}$, we write

$$I(\mathbf{q},t) = \int d\Omega \int d\Omega' \; P(\Omega, t; \Omega', 0) \left\langle \exp\Big(i\mathbf{q}^T \cdot [\mathbf{r}(\Omega) - \mathbf{r}(\Omega')]\Big) \right\rangle_{\Omega_q}, \tag{150}$$

where $\langle \ldots \rangle_{\Omega_q}$ denotes an average over all directions of $\mathbf{q}$. Here $\mathbf{r}$ denotes the position of a "representative" atom with respect to the center of mass. The joint probability density is now decomposed as $P(\Omega, t; \Omega', 0) = P(\Omega_r, t|0,0) P_{eq}(\Omega')$. Since we assume the system to be isotropic, we have

$$P_{eq}(\Omega') = \frac{1}{8\pi^2}. \tag{151}$$

It is now convenient to perform a variable change $\Omega \to \Omega_r$ and to use that $\mathbf{D}(\Omega) = \mathbf{D}(\Omega_r) \cdot \mathbf{D}(\Omega')$. This allows us to write

$$I(\mathbf{q},t) = \int d\Omega_r \, P(\Omega_r, t|0,0) \frac{\sin\big(q|\mathbf{r}(\Omega_r) - \mathbf{r}^{(0)}|\big)}{q|\mathbf{r}(\Omega_r) - \mathbf{r}^{(0)}|}. \tag{152}$$

Denoting the spherical Bessel functions by $j_l(z)$, with $j_0(z) = \sin z/z$, one can invoke the addition theorem for spherical Bessel functions **[51, 52]**,

$$j_0(k\rho) = \sum_{n=0}^{\infty} (2n+1) j_n(k\rho_1) j_n(k\rho_0) p_n(\cos\beta). \tag{153}$$

Here $\rho := \sqrt{\rho_1^2 + \rho_0^2 - 2\rho_1\rho_0\cos\beta}$, and $p_n(x)$ are the Legendre polynomials. To evaluate formula (152) we set $\rho_1 = |\mathbf{r}(\Omega)| = R$, $\rho_0 = |\mathbf{r}^{(0)}| = R$, $\cos\beta = \mathbf{r}_1^T(\Omega) \cdot \mathbf{r}^{(0)}/R^2$. Using $p_n(\cos\beta) = D^n_{00}(\alpha, \beta, \gamma)$ together with the orthogonality of the Wigner functions yields

$$I(\mathbf{q},t) = \sum_{l=0}^{\infty} (2l+1) j_l^2(qR) \exp\Big(-\gamma_r l(l+1)t\Big). \tag{154}$$

To verify that the incoherent intermediate scattering functions fulfills the initial condition $I(\mathbf{q},0) = 1$, one can invoke the theorem $\sum_{l=0}^{\infty}(2l+1)j_l^2(z) = 1$ **[51]**.

Bibliography

[1] W. Doster, S. Cusack, and W. Petry. Dynamical transition of myoglobin revealed by inelastic neutron scattering. *Nature*, 337:754–756, 1989.

[2] L. Cordone, M. Ferrand, E. Vitrano, and G. Zaccai. Harmonic behaviour of trehalose-coated carbon-monoxy-myoglobin at high temperature. *Biophys. J.*, 76:1043–1047, 1999.

[3] M Ferrand, A. J. Dianoux, W. Petry, and J. Zaccai. Thermal motions and function of bacteriorhodopsin in purple membranes: Effects of temperature and hydration studied by neutron scattering. *Proc. Natl. Acad. Sci. USA*, 90:9668–9672, 1993.

[4] B.F. Rasmussen, A.M. Stock, D. Ringe, and G. Petsko. Crystalline ribonuclease a looses function below the dynamical transition at 220 K. *Nature*, 357:423–424, 1992.

[5] R.M. Daniel, J.C. Smith, M. Ferrand, S. Héry, R. Dunn, and J. Finney. Enzyme activity below the dynamical transition at 220K. *Biophys. J.*, 75:2504–2507, 2000.

[6] P. Melchers, E.W. Knapp, F. Parak, L. Cordone, A. Cupane, and M. Leone. Structural fluctuations of myoglobin from normal-modes, Mössbauer spectroscopy, Raman, and absporption spectroscopy. *Biophys. J.*, 70:2092–2099, 1996.

[7] J. Smith. Protein dynamics : Comparison of simulations with inelastic neutron scattering experiments. *Q. Rev. Biophys.*, 24(3):227–291, 1991.

[8] G.R. Kneller, V. Keiner, M. Kneller, and M. Schiller. Nmoldyn, a program package for the calculation and analysis of neutron scattering spectra from MD simulations. *Comp. Phys. Comm.*, 91:191–214, 1995. Full description in report ILL95KN02T, Institut Laue-Langevin, 156 X, F-38042 Grenoble Cedex, France.

[9] T. Rog, K. Murzyn, K. Hinsen, and G.R. Kneller. nMoldyn : A Program Package for a Neutron Scattering Oriented Analysis of Molecular Dynamics Simulations. *J. Comp. Chem.*, 24(5):657–667, 2003.

[10] M. Bée. *Quasielastic Neutron Scattering: Principles and Applications in Solid State Chemistry, Biology and Materials Science*. Adam Hilger, Bristol, 1988.

[11] S.W. Lovesey. *Theory of Neutron Scattering from Condensed Matter*, volume I. Clarendon Press, Oxford, 1984.

[12] G.R. Kneller. Neutron scattering from classical systems: Stationary phase approximation of the scattering law. *Mol. Phys.*, 83(1):63–87, 1994.

[13] L. van Hove. Correlations in space and time and born approximation in systems of interacting particles. *Phys. Rev.*, 93(1):249–262, 1954.

[14] S. Cusack and W. Doster. Temperature dependence of the low frequency dynamics of myoglobin. *Biophys. J.*, 58:248–251, 1990.

[15] W. Doster, S. Cusack, and W. Petry. Dynamical transition of myoglobin revealed by inelastic neutron scattering. *Nature*, 337:754–756, 1989.

[16] J.P. Boon and S. Yip. *Molecular Hydrodynamics*. McGraw Hill, 1980.

[17] A. Rahman, K.S. Singwi, and A. Sjolander. Theory of slow neutron scattering by liquids. I. *Phys. Rev.*, 126(3):986–996, 1962.

[18] H. Frauenfelder, F. Parak, and R.D. Young. Conformational substates in proteins. *Ann. Rev. Biophys. Chem.*, 17:451–479, 1988.

[19] G.R. Kneller, M.-C. Bellissent-Funel, and V. Hamon. Lysozyme in solution under pressure. Technical Report 8-04-286, Institut Laue-Langevin, 2004.
[20] J. Pérez, J.-M. Zanotti, and D. Durand. Evolution of the internal dynamics of two globular proteins from dry powder to solution. *Biophys. J.*, 77:454–469, 1999.
[21] V. Hamon, M.-C. Bellissent-Funel, K. Hinsen, and G.R. Kneller. Quasielastic scattering from lysozyme under pressure - simulation and experiment. Manuscript in preparation.
[22] B. Nystrom and J. Roots. Quasielastic light scattering studies of the pressure-induced denaturation of lysozyme. *Makromol. Chem.*, 185:1441–1447, 1984.
[23] J. Happel and H. Brenner. *Low Reynolds number hydrodynamics*. Noordhoff, Leyden, 1973.
[24] B.J. Berne and R. Pecora. *Dynamic Light Scattering*. Dover Publications, 2000.
[25] A.R. Edmonds. *Angular Momentum in Quantum Mechanics*. Princeton University Press, Princeton, Princeton University Press, Princeton , New Jersey, 1957.
[26] D.M. Brink and G.R. Satchler. *Angular Momentum*. Clarendon Press, Oxford, 1968.
[27] B. Cichocki, B.U. Felderhof, and R. Schmitz. Hydrodynamic interactions between two spherical particles. *PhysicoChemical Hydrodynamics*, 10:383, 1988.
[28] F. Volino and A.J. Dianoux. Neutron incoherent scattering law for diffusion in a potential of spherical symmetry: General formalism and application to diffusion inside a sphere. *Mol. Phys.*, 41(2):271–279, 1980.
[29] J.-M. Zanotti, M.-C. Bellissent-Funel, and J. Parello. Hydration-coupled dynamics in proteins studied by neutron scattering and NMR: The case of typical EF-hand calcium-binding parvalbumin. *Biophysical Journal*, 76:2390–2411, 1999.
[30] J. Fitter, S.A.W. Verclas, R.E. Lechner, H. Seelert, and N.A. Dencher. Function and picosecond dynamics of bacteriorhodopsin in purple membrane and different lipidation and hydration. *FEBS Letters*, 433:321–325, 1998. Habil.
[31] P. Langevin. Sur la théorie du mouvement brownien. *C. Rendus Acad. Sci. Paris*, 146:530–533, 1908.
[32] N.G. van Kampen. *Stochastic Processes in Physics and Chemistry*. North Holland, Amsterdam, revised edition, 1992.
[33] H. Risken. *The Fokker-Planck Equation*. Springer Series in Synergetics. Springer, Berlin, Heidelberg, New York, 2nd reprinted edition, 1996.
[34] C.W. Gardiner. *Handbook of Stochastic Methods*. Springer Series in Synergetics. Springer, Berlin, Heidelberg, New York, 2nd edition, 1985.
[35] G.R. Kneller. Inelastic neutron scattering from damped collective vibrations of macromolecules. *Chem. Phys.*, 261(1+2):1–24, 2000. Special volume "Condensed Phase Structure and Dynamics : A combined neutron scattering and molecular modelling approach".
[36] D.A. McQuarrie. *Statistical Mechanics*. Harper's Chemistry Series. Harper Collins Publishers, 1976.
[37] G. Zaccai. How soft is a protein? A protein dynamics force constant measured by neutron scattering. *Science*, 288:1604–1607, 2000.
[38] B.R. Brooks, R.E. Bruccoleri, B.D. Olafson, D.J. States, S. Swaminathan, and M. Karplus. Charmm: A program for macromolecular energy, minimization, and dynamics calculations. *J. Comp. Chem.*, 4:187–217, 1983.
[39] A.D. MacKerell, D. Bashford, M. Bellott, R.L. Dunbrack, J.D. Evanseck, M.J. Field, S. Fischer, J. Gao, H. Guo, S. Ha, D. J. McCarthy, L. Kuchnic, K. Kuczera, F.T.K. Lau, C. Mattos, S. Michnick, T. Ngo, D.T. Nguien, B. Prudhom, W.E. Reicher, B. Roux, M. Schlenkirch, J.C. Smith, R. Stote, J. Straub, M. Watanabe, J. Wiokiewicz-Kuczera, D. Yin, and M. Karplus. All-atom empirical potential for molecular modeling and dynamics studies of proteins. *J. Phys. Chem. B*, 102:3586–3616, 1998.
[40] BIOMOS b.v., Laboratory of Physical Chemistry, ETH Zurich. *The GROMOS96 users manual*.

[41] W.D. Cornell, P. Cieplak, C.I. Bayly, I.R. I.R. Gould, K.M. Merz Jr, D.M. Ferguson, D.C. Spellmeyer, T. Fox, J.W. Caldwell, and P.A. Kollman. A second generation force field for the simulation of proteins and nucleic acids. *J. Am. Chem. Soc*, 117:5179, 1995.

[42] L. Verlet. Computer "experiments" on classical fluids. Thermodynamic properties of Lennard-Jones molecules. *Phys. Rev.*, 159(1):98–103, 1967.

[43] G.R. Kneller and J.C. Smith. Liquid-like side-chain motions in myoglobin. *J. Mol. Biol.*, 242:181–185, 1994.

[44] K. Hinsen, A.-J. Petrescu, S. Dellerue, M.C. Bellissent-Funel, and G.R. Kneller. Harmonicity in slow protein dynamics. *Chem. Phys.*, 261(1+2):25–38, 2000. Special Issue "Condensed Phase Structure and Dynamics: A combined neutron scattering and molecular modelling approach".

[45] R. Zwanzig. *Statistical Mechanics of Irreversibility*, pages 106–141. Lectures in Theoretical Physics. Wiley-Interscience, New York, 1961.

[46] G.R. Kneller and K. Hinsen. Fractional brownian dynamics in proteins. Submitted.

[47] G.R. Kneller and K. Hinsen. Computing memory functions from Molecular Dynamics simulations. *J. Chem. Phys.*, 115(24):11097–11105, 2001.

[48] M.F. Shlesinger, G.M. Zaslavsky, and J. Klafter. Strange Kinetics. *Nature*, 363:31–37, 1993.

[49] W.G. Glöckle and T.F. Nonnenmacher. A fractional calculus approach to self-similar protein dynamics. *Biophys. J.*, 68:46–53, 1995.

[50] J.G. Kirkwood. *Macromolecules*, chapter Statistical mechanics of irreversible processes in polymer solutions, pages 56–64. John Gamble Kirkwood Collected Works. Gordon and Breach Science Publishers, 1967.

[51] M. Abramowitz and I.A. Stegun (eds.). *Handbook of Mathematical Functions*. Dover Publications, New York, 1972.

[52] A. Sommerfeld. *Partielle Differentialgleichungen in der Physik*. Verlag Harry Deutsch, Thun, Frankfurt/M., 1978.